Nucleic Acids Research, 2024, **52**, 10897–10917
https://doi.org/10.1093/nar/gkae714
Advance access publication date: 21 August 2024
Gene regulation, Chromatin and Epigenetics

Unexpected nuclear hormone receptor and chromatin dynamics regulate estrous cycle dependent gene expression

Wendy N. Jefferson [1,†], **Tianyuan Wang** [2,†], **Elizabeth Padilla-Banks** [1] and **Carmen J. Williams** [1,*]

[1]Reproductive & Developmental Biology Laboratory, Research Triangle Park, NC 27709, USA
[2]Biostatistics and Computational Biology Branch, National Institute of Environmental Health Sciences, NIH, Research Triangle Park, NC 27709, USA

[*]To whom correspondence should be addressed. Tel: +1 984 287 4313; Fax: +1 301 480 2732; Email: williamsc5@niehs.nih.gov
[†]The first two authors should be regarded as Joint First Authors.

Abstract

Chromatin changes in response to estrogen and progesterone are well established in cultured cells, but how they control gene expression under physiological conditions is largely unknown. To address this question, we examined *in vivo* estrous cycle dynamics of mouse uterus hormone receptor occupancy, chromatin accessibility and chromatin structure by combining RNA-seq, ATAC-seq, HiC-seq and ChIP-seq. Two estrous cycle stages were chosen for these analyses, diestrus (highest estrogen) and estrus (highest progesterone). Unexpectedly, rather than alternating with each other, estrogen receptor alpha (ERα) and progesterone receptor (PGR) were co-bound during diestrus and lost during estrus. Motif analysis of open chromatin followed by hypoxia inducible factor 2A (HIF2A) ChIP-seq and conditional uterine deletion of this transcription factor revealed a novel role for HIF2A in regulating diestrus gene expression patterns that were independent of either ERα or PGR binding. Proteins in complex with ERα included PGR and cohesin, only during diestrus. Combined with HiC-seq analyses, we demonstrate that complex chromatin architecture changes including enhancer switching are coordinated with ERα and PGR co-binding during diestrus and non-hormone receptor transcription factors such as HIF2A during estrus to regulate most differential gene expression across the estrous cycle.

Graphical abstract

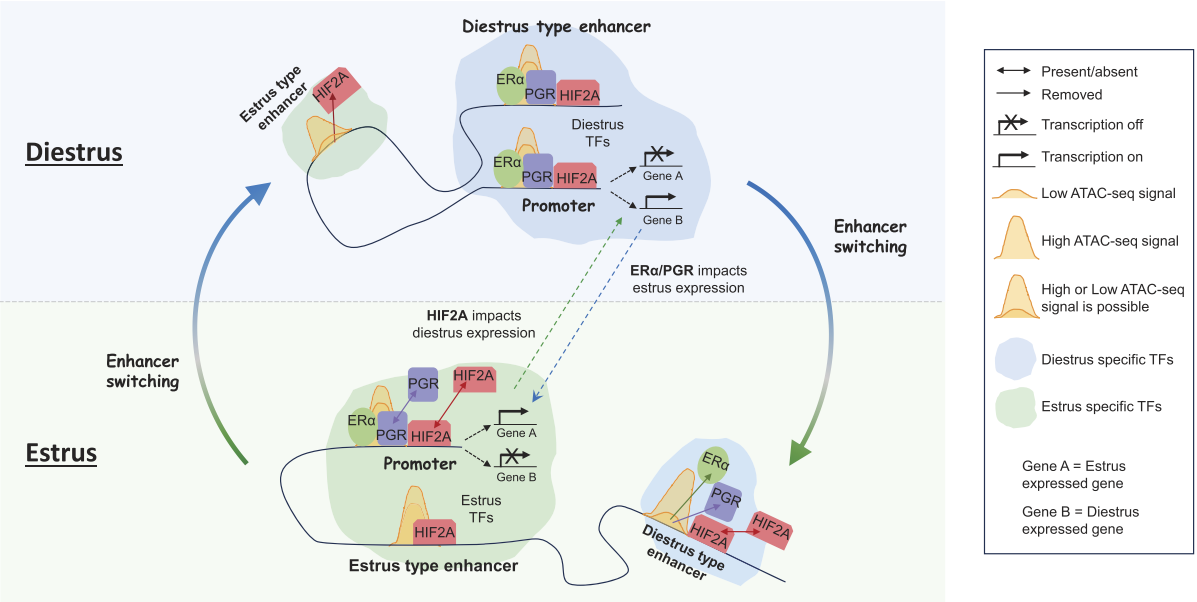

Introduction

Estrogen and progesterone play critical roles in driving uterine responses essential for pregnancy. Estrogen generally regulates gene expression to cause cell proliferation while progesterone counters this activity and induces cell differentiation (1). In the adult mouse, these changes occur in a cyclic manner over 4–5 days of the estrous cycle to continually prepare for establishment of pregnancy. The highest levels of estra-

Received: January 15, 2024. **Revised:** June 27, 2024. **Editorial Decision:** July 27, 2024. **Accepted:** August 6, 2024
Published by Oxford University Press on behalf of Nucleic Acids Research 2024.

diol occur during diestrus and proestrus and the highest levels of progesterone occur during estrus and metestrus, though both hormones are in circulation throughout the cycle (2,3). It is unknown how the epigenome responds to these dynamic changes in hormonal cues to cause gene expression changes that control uterine cell fates.

A central dogma has been that steroid hormone activity in the uterus is largely executed by hormone binding to its corresponding receptor, followed by receptor-DNA binding at specific 'hormone response elements' in regions of accessible chromatin (4,5). For example, estrogen receptor alpha (ERα) binds to estrogen response elements (ERE) and the progesterone receptor (PGR) binds to progesterone response elements (PRE). Of note, the PRE is not specific for PGR binding because the androgen, glucocorticoid, and mineralocorticoid receptors also bind the same sequences (6–8). Hormone-receptor-DNA interactions, together with associated co-activators or co-repressors, impact nearby gene transcription required for cellular responses to hormones. This stepwise series of events was largely determined using either *in vitro* systems or ovariectomized (ovx) mice treated with estradiol or progesterone alone (4,9). There is a gap in our knowledge of how steroid hormones regulate physiological responses in living tissues *in vivo*.

ERα binding to EREs often occurs in chromatin regions that are already accessible prior to ligand binding to the receptor, suggesting that open chromatin is more favorable to ERα binding than closed chromatin (10). Closed chromatin also can become accessible to ERα binding through pioneering transcription factors such as FOXA1, GATA3 and PBX1 (11). However, there is also evidence from cell lines that ERα can bind inaccessible chromatin regions as defined by assay for transposase-accessible chromatin with sequencing (ATAC-seq) (8). In the uterus, ERα and PGR also bind DNA both in the absence and presence of hormone (6,7). These findings challenge the universality of the 'hormone-receptor-DNA interaction at accessible chromatin' paradigm as a driver of gene expression changes.

Here, we focus on how ERα regulates uterine gene expression changes in the complex physiological setting of cycling adult female mice. Chromatin accessibility, ERα binding, PGR binding, and 3D chromatin structure were measured during two stages of the estrous cycle: diestrus, when estrogen levels are high, and estrus, when progesterone levels are high. We find that there are estrous cycle dependent changes in chromatin accessibility as well as constitutively open chromatin, both of which are associated with changes in ERα and PGR occupancy. Surprisingly, while PGR binding to DNA is largely ERα-independent, almost all ERα binding is accompanied by PGR binding. We show distinct differences between how genes are regulated during estrus and diestrus, and a novel role for HIF2A during estrus.

Materials and methods

Animals

All animals used in this study were under protocol number RDBL07-38 that was approved by the NIEHS Animal Care and Use Committee (ACUC). Outbred CD-1 female mice were weaned at 22 days of age, housed five per cage, fed NIH-31 mouse chow and given water ad libitum. At 2 months of age, all mice were euthanized by CO_2 asphyxiation and death insured by thoracotomy; no other treatments or procedures were administered. Uteri were collected at 2 months of age and immediately frozen on dry ice and then stored at −80°C until further use. For estrous cycle staging, vagina was collected, fixed in cold 10% neutral buffered formalin, and changed to cold 70% ethanol 48 h later. Vaginal tissues were embedded in paraffin, sectioned at 6 microns and stained with hematoxylin and eosin for estrous cycle staging as described previously (12). Uteri from female mice in diestrus when estrogen is highest or estrus when progesterone is highest were selected for further analysis.

Immunohistochemistry

Female reproductive tract tissues were collected from 2-month-old mice that were then identified as being in diestrus and estrus by vaginal histology staging (n = 3–4 mice per group). Uterine tissue sections were deparaffinized, hydrated and endogenous peroxidases quenched with hydrogen peroxide (3%) for 15 min at RT. Antigen retrieval was performed using a NxGen Decloaker (Biocare Medical) with 1× citrate buffer, pH 6.0 for 15 min (Biocare Medical). Endogenous peroxidases were quenched with 3% hydrogen peroxide for 15 min. For ERα immunohistochemistry (IHC), sections were blocked with mouse on mouse (M.O.M.) IgG blocking solution for 1 h at room temperature (RT) followed by 2.5% RTU normal horse serum for 5 min at RT (ImmPress kit, Vector Laboratories). For PGR IHC, sections were blocked with 2.5% normal horse serum for 20 min at RT (Vector Laboratories). For ERα IHC, sections were incubated with mouse monoclonal anti-human ERα, clone 6F11 (Bio-Rad, Cat# MCA1799T, Lot# 159277, 1 mg/ml) diluted 1:500 in Van Gogh Yellow diluent (Biocare Medical) for 30 min at RT. Mouse IgG1 Isotype control serum (BD Biosciences, Cat# 557273, Lot# 8299643, 0.5 mg/ml) was applied at an equivalent dilution as a negative control. For PGR IHC, sections were incubated with monoclonal rabbit anti-PGR antibody (Cell Signaling cat#8757, Lot# 3, 0.62 mg/ml) diluted 1:1000 in Van Gogh Yellow diluent for 1 h at RT. Negative control tissue section received normal rabbit IgG (Millipore cat#N101, Lot#3939454, 0.1 mg/ml) diluted to match primary antibody concentration. For ERα IHC, sections were incubated with Vector ImmPress M.O.M. HRP Polymer (Vector Laboratories) for 10 min at RT. For PGR IHC, Vector ImmPress anti-rabbit IgG Polymer (Vector Labs Cat#MP-7401) was applied for 15 min at RT. Antigen–antibody complexes were visualized using 3-diaminobenzidine (DAB) chromogen (DakoCytomation) for 6 min at RT. Tissue sections were counterstained with hematoxylin, dehydrated through graded ethanol series, cleared in xylene and coverslipped.

Image analysis and quantification by Visiopharm machine learning algorithms

Images were captured using Aperio ImageScope v. 12.4.3.5008 (Leica Biosystems). All images were imported into the Visiopharm image analysis software platform (Visiopharm), regions of interest were manually drawn on one uterine horn and the muscle layer was manually delineated from the stroma (Supplementary Figure S1A). We used the Visiopharm algorithm, DeepLab convolution neural network (CNN) at low resolution (10X) to detect the tissue compartments: glandular epithelium, luminal epithelium, stroma and muscle (Supplementary Figure S1B). A second

Visiopharm algorithm was trained to segment and separate the cell nuclei using DeepLab CNN at 20X resolution; nuclei detection was restricted to 5–20 μm^2. Each nucleus was then classified as positive or negative for DAB chromogen and assigned an intensity level of 1+, 2+ or 3+ (1+ being the least and 3+ being the most) (Supplementary Figure S1C). The percent of nuclei in each category was then calculated across all images and markers. Using GraphPad Prism version 9.4.1, a one-way ANOVA was performed followed by Sidak's multiple comparisons test using the percent cells in each category (diestrus versus estrus as select pairs); statistical significance is reported for $P \leq 0.05$.

RNA isolation and RNA-seq

Total RNA was isolated from ∼20 mg uterine tissue from 2-month-old adults (diestrus and estrus) using the Qiagen RNeasy kit (Qiagen) and the RNase free DNase clean up kit (Qiagen) ($n = 1$ mouse per sample; 4 samples per group). Quality of RNA was determined using a Bioanalyzer and 1 μg of RNA was used for making libraries for sequencing using the TruSeq RNA kit (Illumina). Libraries were sequenced on a NextSeq 500 (Illumina) at a depth of >30 million reads per sample. Raw reads (76 bp, paired-end) were initially processed by filtering with average quality scores >20. One library in the estrus group did not have high quality reads and was omitted from further analysis. The reads passing the filter were aligned to the mouse reference genome (mm10; Genome Reference Consortium Mouse Build 38 from December 2011) using TopHat version 2.0.4 (13). Expression values of RNAseq were represented as FPKM (fragments per kilobase of exon per million fragments). Differential expression was calculated using Cufflink version 2.2.1 (14). Differentially expressed genes (DEGs) were defined as absolute fold change ≥1.5, adjusted *P*-value <0.05 and having average FPKM ≥1 in at least one of the groups. Functional analysis of gene lists was performed using the 'enrichGO' function of the clusterProfiler R package (15).

Re-analysis of single cell RNA-seq from uteri of intact cycling mice

In a recent study, single cell RNA-seq was performed on uteri from young adult C57BL/6J mice (14–18 weeks of age) (16). We downloaded the 10× Genomics processed data files from ArrayExpress (E-MTAB-11491); diestrus samples (Ind002, Ind008, Ind016) and estrus samples (Ind003, Ind009, Ind014). We used Seurat (version 3.6.3) to perform normalization, scaling, and clustering analysis of the merged dataset in each group (17). The FeaturePlot function in the Seurat package was used to generate gene expression plots for individual genes and dual feature plot for two genes at the same time. For the dual feature plots, expression was converted to either expressed (>0) or not expressed (0) to visualize individual cells that had overlapping expression of the two genes of interest. Cell types were identified using gene expression markers from a previous study of single RNA-seq on 12-month old control CD-1 uteri (18).

Chromatin immunoprecipitation sequencing (ChIP-seq)

Uteri collected and frozen from adult mice (diestrus and estrus, pools of 6–8 uteri with 150–200 mg per sample; $n = 1$ pooled sample per group for all ChIP-seq analyses) were sent to Active Motif for ChIP-seq using the following antibodies: ERα (Santa Cruz; cat# sc-543), PGR (Active Motif; cat#61023), and HIF2A (Active Motif, cat# 39665). Raw ChIP-seq reads (76 bp, single-end) were filtered with average quality scores greater than 20. The reads were aligned to the mouse reference genome (mm10) using Bowtie version 1.1.2 with unique mapping and up to 2 mismatches for each read (-m 1 -v 2) (19). Duplicated reads with identical sequences were removed using the 'MarkDuplicates' function of Picard tools. The retained read alignments were extended to 300 bases. Normalization of sequencing depth across each ChIP-seq dataset was achieved by down sampling to the same number of uniquely mapped reads per sample; a single input sample for diestrus and estrus was generated to ensure antibody specificity but not used for normalization. To visualize the read coverage, bigWig files were generated from the bedgraph files of each sample using bedGraphToBigWig (20). These bigWig files were displayed as custom tracks on the UCSC genome browser. Peaks were identified using MACS2 with a cutoff of adjusted *P*-value <0.0001 (21). Genome distribution was determined using PAVIS with default settings.

ATAC-seq

Uteri were collected from adult mice and frozen on dry ice (diestrus and estrus, pools of 3–4 mice, 20 mg per sample; $n = 2$ pooled samples per group). Uteri were pulverized on dry ice and nuclei extracted and libraries prepared for ATAC-seq using previously published procedures (22,23). Briefly, nuclei were extracted using OMNI-ATAC Resuspension Buffer (RSB) (23) and a chilled glass dounce. Debris was filtered out using CellTrix 100 μm followed by CellTrix 30 μm filters (Sysmex, Lincolnshire, IL). Nuclei were counted using a hemacytometer and 50 000 nuclei were used in the transposition reaction as described previously (22). Sequencing was performed on a NextSeq 500 (Illumina). Raw reads (50 bp, paired-end) were processed by trimming adaptors and filtering with average quality scores greater than 20 by Trim Galore version 6.7 (https://github.com/FelixKrueger/TrimGalore). The reads passing the initial processing were aligned to the mouse reference genome (mm10) using bowtie version 1.1.2 with unique mapping and up to 2 mismatches for each read (-m 1 -v 2). After removing the reads mapped to mitochondrial DNA and the duplicated reads, the uniquely mapped deduplicated reads in each sample were normalized by down-sampling to 100 million. Only the first 9 bp of each read were used for downstream analyses. The open chromatin regions were first identified by MACS2 with a cutoff of adjusted *P*-value 0.0001, followed by merging genomic intervals within 100 bp of each other (21).

Identification of nearest gene and motif analysis

The gene associated with each peak was predicted by searching the transcription start site (TSS) of nearby genes within a 100 Kb range using 'annotatePeaks.pl' function of Hypergeometric Optimization of Motif EnRichment (HOMER) motif discovery tool (24). HOMER's findMotifsGenome.pl' function was used for motif enrichment analysis of given peak ranges. For the differential ATAC-seq motif analysis, there was a 4-fold difference in the number of diestrus and estrus specific differential ATAC-seq locations that led us to perform a down-sampling of the larger estrus group to match the smaller diestrus group. The motifs for PGR, androgen receptor (AR)

and glucocorticoid receptor (GR) are identical and were combined and reported as PGR/AR/GR.

Differential region identification

Differential regions of any pair of ChIP-seq or ATAC-seq samples were identified using MEDIPS software (Model-based Exploration of DiPloid Sequencing data) with window size of 250 bp (25). The main function used was 'medips.meth with parameter of p.adj = 'fdr' and diff.method = 'edgeR'. Each differential region was defined as the genomic interval with at least 2-fold differences in mapped read count and adjusted *P*-value ≤0.01.

High-throughput chromosome conformation capture (HiC-seq)

Uteri were collected from adult mice and frozen on dry ice (diestrus and estrus, pools of 3–4 mice, 20 mg per sample; $n = 1$ pooled sample per group). Uteri were pulverized on dry ice and DNA extracted using Qiagen Blood and Tissue kit. HiC libraries were prepared from 1 μg of DNA per sample using the Arima HiC kit following manufacturer's instructions. Sequencing was performed on a NovaSeq 6000 (Illumina). The raw reads (151 bp, paired-end) generated from HiC libraries were mapped to the mouse reference genome (mm10), truncated and deduplicated using HiCUP version 0.7.1 (26). The uniquely mapped di-tags passing quality filtering with distance larger than 10 kb were used for downstream analysis. Chromatin loops were identified using the 'hiccups' function of Juicer version 1.8.9 with default parameters (27). The classification of common and differential loops was based on a loop's presence in diestrus and estrus samples.

Rapid immunoprecipitation mass spectrometry of endogenous proteins (RIME)

To determine proteins that were in complex with ERα, frozen uteri from 2-month-old diestrus and estrus mice (pool of 10–15; 800 mg) were sent to Active Motif for Rapid Immunoprecipitation Mass spectrometry of Endogenous proteins (RIME) assays using ERα antibody (Santa Cruz; cat# sc-543). Each pooled sample was split into two and RIME performed; peptides identified in at least one replicate per group were included as a protein associated with ERα. Details of this procedure can be found in Mohammed *et al.* (28). There was less pull down of ERα in the estrus sample (26 peptides detected) compared to the diestrus sample (32.5 peptides detected) so graphical representation of counts of all peptides in diestrus were normalized to reflect that difference.

Results

ERα binding is estrous cycle stage dependent with distinct transcription factor landscapes

To determine the dynamics of ERα binding to chromatin over the estrous cycle, we performed ERα ChIP-seq on uterine tissue samples at 2 months age during diestrus and estrus. Genomic distribution of ERα ChIP-seq peaks in adult cycling mice was in agreement with ERα binding locations observed in the uterus of ovariectomized (ovx) mice with and without estradiol treatment (29). In the current study, ERα binding sites were distributed similarly between diestrus and estrus with most occurring at intergenic regions (diestrus, 44.1%; estrus, 38.1%) and introns (diestrus, 33.6%; estrus, 32.0%) (Supplementary Figure S2A). The promoter region also exhibited substantial binding that was not different between diestrus and estrus [diestrus, 13.2% upstream of the TSS (−5 kb) and 5.3% at the 5′-UTR; estrus, 15.4% upstream of the TSS and 8.8% at the 5′-UTR]. Differential analysis of ERα ChIP-seq signal between estrus and diestrus (≥2-fold) identified 21 113 differential ERα binding regions (DERs; 9215 gain and 11 898 loss in estrus relative to diestrus) (Figure 1A and Supplementary Table S1A, B). We define regions where ERα was present at higher levels in diestrus as 'diestrus specific' and regions where ERα was present at higher levels in estrus as 'estrus specific'. There was a striking lack of ERα binding during diestrus (below background) in estrus specific ERα binding locations; this ERα binding pattern has been observed previously in primary liver cells (30). The absence of ERα (below background) was much less prevalent in diestrus specific ERα binding locations. As expected, the ERα binding motif (estrogen response element, ERE) was one of the most highly enriched motifs at both stages of the cycle; however, the enrichment was ∼10-fold greater in diestrus than estrus (Figures 1B, C; Supplementary Table S1C, D). There were 90 unique enriched motifs (107 total) at diestrus specific ERα binding sites and 19 unique (20 total) at estrus specific locations (Figure 1C and Supplementary Figure S2B; Supplementary Table S1C-D). The motif for PGR/AR/GR was found exclusively in diestrus specific ERα binding regions (Figures 1C and Supplementary Figure S2B; Supplementary Table S1C-D). Diestrus specific motifs also included FOXA1, FOXA2, SOX2/3/4/6/17, HOXA9/B4/C9/D13, GATA1/2/3/4 and STAT1/3/4/5. FOXO1 was found in both diestrus and estrus but was 3-fold more enriched in diestrus than estrus (Figure 1C).

To test if the enriched motifs were documented binding sites for the corresponding transcription factors, we compared the DERs to published uterine ChIP-seq datasets available from pregnant mice at gestational day 3.5 for FOXO1, FOXA2, PGR and GATA2 (6,31–33). GATA2 and PGR had the most robust overlap, binding at 36% and 15% of diestrus specific DERs, respectively (Figure 1D). Consistent with the DER motif analysis, GATA2, PGR and FOXA2 had far less overlap with estrus specific DERs. FOXO1 had very low overlap with ERα at DERs but the overlap was still higher at diestrus than estrus. Robust increases in ERα ChIP-seq levels were observed at FOX1, FOXA2, GATA2 and PGR ChIP-seq peaks at diestrus specific DER locations (Figure 1E). In contrast, there were only minimal increases in ERα binding at transcription factor peaks at estrus-specific DER locations. Together with the DER motif analysis, these data suggest that specific transcription factors function combinatorially with ERα in an estrous cycle stage specific manner.

PGR binding is dynamic and coordinated with ERα binding across the estrous cycle

The preferential overlap of PGR motifs with diestrus specific compared to estrus specific DERs led us to test whether PGR was bound at these sites. PGR binding regions were determined by performing PGR ChIP-seq on the same diestrus and estrus samples used for ERα ChIP-seq. Genomic distribution of PGR ChIP-seq peaks was similar to the distribution observed in ovx mice with and without progesterone (Supplementary Figure S2A) (6,34). In the current study, PGR

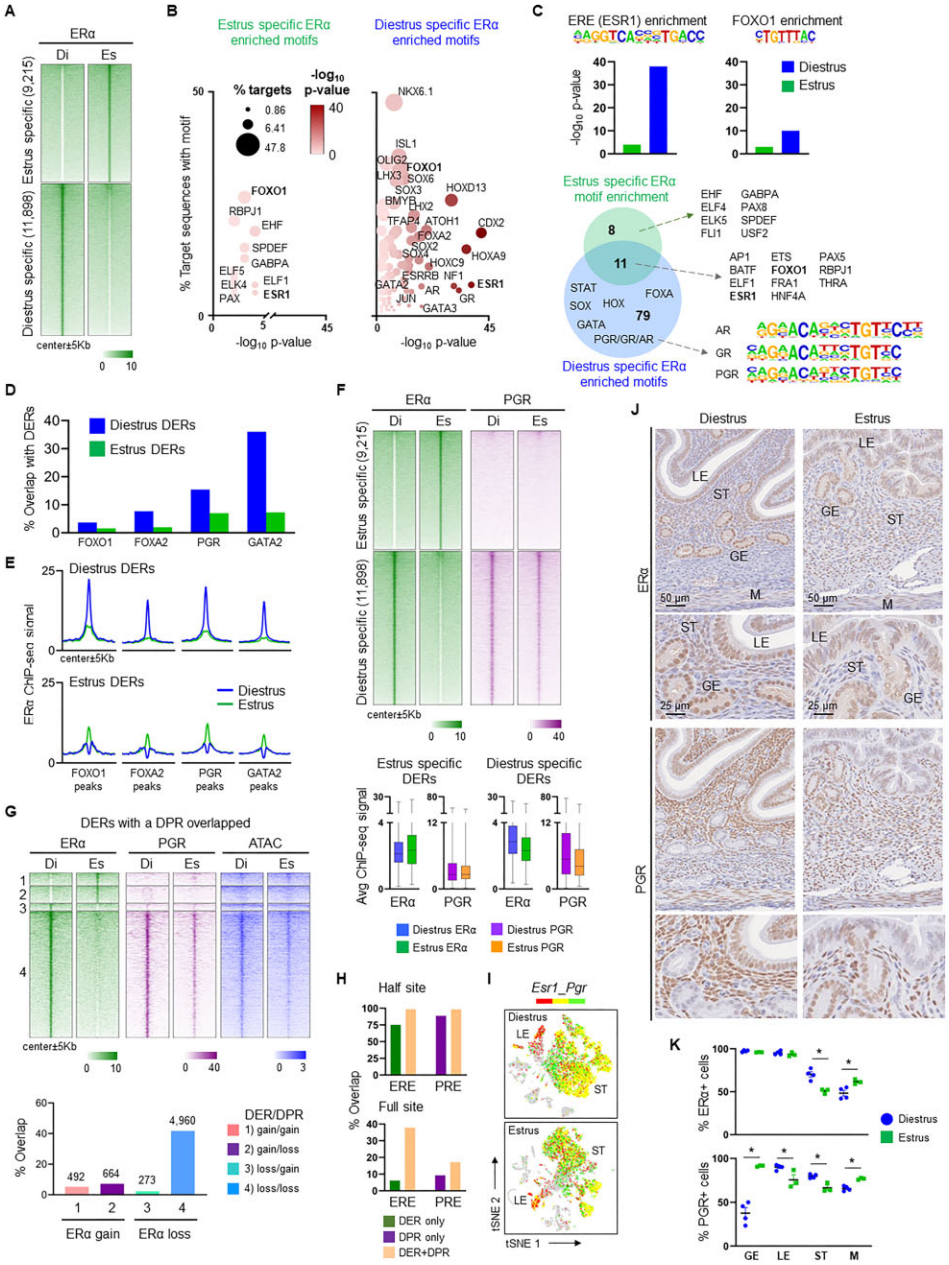

Figure 1. Diestrus specific ERα binding occurred at TF rich locations including PGR while estrus specific ERα binding occurred in TF deserts. (**A**) Heatmaps displaying ChIP-seq signal of differential ERα regions (DERs) ±2-fold between diestrus and estrus (loss and gain defined by estrus versus diestrus). (**B**) Bubble plots of motif enrichment for diestrus and estrus specific DERs. Size of bubble indicates the percent of target sequences with each motif enriched in estrus or diestrus specific ERα binding locations. Color scale indicates $-\log_{10}P$-value. Select motifs are indicated; FOXO1 and ESR1 are in bold for reference. (**C**) Graphs of ERE and FOXO1 motif enrichment using $-\log_{10}P$-values. Venn diagram of motifs enriched in diestrus or estrus specific DERs (numbers of motifs and select motifs are indicated). Motifs for PGR, GR and AR are highly similar and are considered as one motif. (**D**) Percent overlap of DERs (gain or loss) with previously published datasets of FOXA2, FOXO1, GATA2 or PGR ChIP-seq binding locations in the uterus of pregnant mice on gestation day 3.5; data taken from (6,32–34). (**E**) Metaplots of ERα ChIP-seq signal from diestrus and estrus at FOXA2, FOXO1, GATA2 or PGR ChIP-seq binding locations from panel D. (**F**) Heatmaps displaying ChIP-seq signal of DERs from Figure 1A and corresponding PGR ChIP-seq signal in that location. Box and whisker plots show the average ERα and PGR ChIP-seq signal from heat maps above (average of averages = black line across each box) and the maximum and minimum signal for each box. All heatmaps are organized from highest signal to lowest signal of ERα in estrus. Heatmaps are plotted using the center of the peak ±5 kb. Intensity of ChIP-seq signal (reads mapped to each bin of 100 bp) is indicated by color intensity for each heatmap. (**G**) Heatmaps of diestrus and estrus specific DERs that overlap diestrus and estrus specific DPRs (top) split into four categories indicated in bar graph legend (bottom). DER/DPR gain = estrus > diestrus; DER/DPR loss = diestrus > estrus. ATAC-seq signal is also plotted in these same locations for reference. Bar graph plotted as percent of overlap with DER gain for categories 1 and 2 and DER loss in categories 3 and 4. Numbers above the bars are the number of overlapping regions in each comparison. (**H**) Graph of the % overlap of DERs alone, DPRs alone and DERs that also have a DPR (DERs + DPR) with half site EREs and PREs (top) or full site EREs and PREs (bottom). (**I**) tSNE plots of single cell RNA-seq data from the uteri of 14–18 week old C57BL/6J mice during diestrus ($n = 3$ mice combined; top) and estrus ($n = 3$ mice combined; bottom); data taken from (16). (**J**) IHC of ERα and PGR in serial uterine sections from diestrus and estrus; representative sections shown. Scale bar is indicated in ERα IHC and applies to corresponding PGR IHC panels below. LE = luminal epithelium; GE = glandular epithelium; ST = stroma; M = muscle. (**K**) Image analysis quantification of ERα and PGR IHC during diestrus ($n = 4$) and estrus ($n = 3$). Each dot represents an individual mouse. Data is presented as the percentage of either ERα or PGR positive cells in each tissue compartment indicated in panel (J).

ChIP-seq peaks were distributed across the genome in a pattern similar to ERα ChIP-seq peaks and were not different between diestrus and estrus. To determine the extent of PGR coordination with ERα specifically in locations where ERα binding was dynamically changing across the cycle, PGR ChIP-seq signal was plotted at DERs (Figure 1F). At estrus specific DERs, there was a striking lack of PGR occupancy in either diestrus or estrus. In contrast, diestrus specific DERs had coordinate PGR binding with ERα, with decreases in binding of both receptors during estrus. To determine the extent of this coordinated loss, an analysis of differential PGR regions (DPRs) was performed, and these data were overlapped with DER gain and loss (Figure 1G and Supplementary Tables S1E-F). There was < 8% overlap of all categories except the DER loss/DPR loss category, with 42% overlap. ATAC-seq signal was also plotted in these DER/DPR overlapped locations and showed the highest signal in the DER loss/DPR loss group during diestrus, confirming accessibility is coordinated with ERα/PGR association.

To determine if the DNA sequence influenced ERα/PGR co-binding, the presence of half site and full site EREs and PREs was assessed. Almost all ERα/PGR co-bound locations had ERE and PRE half sites compared to 75% of ERα bound alone having an ERE half site and 89% of PGR bound alone having a PRE half site (Figure 1H). Interestingly, there was a 6-fold increase in full site EREs at ERα/PGR co-bound locations compared to ERα bound alone (Figure 1H). There was only a 2-fold increase in PREs at these co-bound locations compared to PGR alone, suggesting EREs may be more influential in binding the two receptors in these locations. These data indicate that ERα and PGR binding at DERs are highly coordinated at full site EREs during diestrus at accessible chromatin and that they are dynamically lost together during estrus.

To determine if a change in ERα or PGR expression levels or cellular localization over the course of the estrous cycle could explain the differences in chromatin binding, we first examined *Esr1* and *Pgr* mRNA expression from a published dataset of single cell RNA-seq from adult uterus during diestrus and estrus (16). We generated tSNE plots of cells from combined diestrus samples ($n = 3$) and combined estrus samples ($n = 3$) showing large populations of stromal cells (*Col6a4* as a marker) and epithelial cells (*Epcam* as a marker); very few glandular epithelial cells (*Foxa2* as a marker) or muscle cells (*Myh11* as a marker) were present in these samples (Supplementary Figure S3) (18). Dual feature plots of *Esr1* and *Pgr* showed very high overlap in stromal and epithelial cells in both diestrus and estrus samples, clearly demonstrating individual cells expressed both of these receptors (Figures 1I and Supplementary Figure S3).

We next performed ERα and PGR immunohistochemistry in serial uterine tissue sections from diestrus and estrus mice to determine estrus cycle dependent ERα and PGR protein expression patterns (Figure 1J and Supplementary Figure S4). ERα was robustly expressed and did not differ visually in the glandular or luminal epithelium between diestrus and estrus (Figure 1J and Supplementary Figure S4). This impression was confirmed by formal image analysis with >90% of luminal and glandular epithelial cells expressing ERα; the highest expression level observed was in glandular epithelial cells during diestrus (Supplementary Table S2A; Figures 1K and Supplementary Figure S4-Supplementary Figure S5). PGR expression was much more dynamic in these two cell types with PGR expression in > 90% of glandular epithelial cells during estrus and expression in >90% of luminal epithelial cells during diestrus (Supplementary Table S2B; Figure 1K and Supplementary Figure S4-Supplementary Figure S5). Hence, most glandular epithelial cells have both ERα and PGR during estrus and most luminal epithelial cells have both receptors during diestrus. In the stroma, many cells expressed ERα and PGR during diestrus, but fewer did so during estrus (Figure 1K). Muscle cells had similar percentages of ERα and PGR positive cells as stromal cells, but the pattern was reversed, with higher percentages during estrus compared to diestrus. The overall high percentages of uterine cells that express ERα and PGR at the protein level make it very likely that many cells co-express both ERα and PGR.

Chromatin accessibility and TF occupancy changes across the estrous cycle

ATAC-seq was performed to determine how the dynamic differences in ERα and PGR binding to chromatin across the estrous cycle were related to changes in chromatin accessibility. Analysis of differential ATAC regions (DARs) between diestrus and estrus revealed ∼4-fold more estrus specific DARs (9958) relative to diestrus specific DARs (2454) (Figure 2A and Supplementary Table S3A, B). At genomic locations identified as estrus specific DARs, the ERα ChIP-seq signal showed overall low occupancy that was no different in diestrus and estrus uteri. In contrast, PGR occupancy at estrus specific DARs was readily observed in diestrus and was lower in estrus. At genomic locations identified as diestrus specific DARs, both ERα and PGR ChIP-seq signals were higher in diestrus and lower in estrus, directly correlating with ATAC-seq signals.

A motif analysis of the diestrus and estrus specific DARs showed striking differences between these two groups (Supplementary Table S3C–E). There were 103 enriched motifs (86 unique) for down-sampled estrus specific DARs and 89 enriched motifs (77 unique) for diestrus specific DARs (Figure 2B and Supplementary Figure S6; Supplementary Table S3C-F). There were 26 enriched motifs found in diestrus but not in estrus DARs, including PGR/AR/GR, SOX17 and FOXA1. PGR ChIP-seq was consistent with this finding because there was higher signal in diestrus specific DARs compared to estrus specific DARs (Figure 2A). The 47 motifs in common included ERα, ATF, HOXA9, STAT1/3/4/5, SOX2/3/4/6, FOXA2 and FOXO1 (Figure 2B and Supplementary Figure S6 and Supplementary Tables S3C, S3E–F). Notably, ERα enrichment was very low for both diestrus and estrus specific DARs ($P = 1.00e\text{-}4$ for both). Motifs that were only enriched in estrus specific DARs included ELF, ELK, VDR, HOXA2/B4/C9, PAX3/5/8, HIF1A and HIF2A (Figure 2B, Supplementary Tables S3C, S3E and S3F). HIF2A was of particular interest because it is required for uterine function during early embryo implantation and is regulated by estrogen under progesterone primed conditions (35,36). For these reasons, we selected HIF2A for further investigation of its potential role in estrous cycle dependent accessibility. HIF2A ChIP-seq in diestrus and estrus samples confirmed that HIF2A is more highly associated with estrus specific compared to diestrus specific DARs (Figure 2C).

To determine the degree to which changes in ERα, PGR and HIF2A binding were associated with changes in chromatin accessibility, we plotted heatmaps of the ATAC-seq signal corresponding to DER gain/loss, DPR gain/loss or HIF2A gain/loss (Figure 2D and Supplementary Table S1A, B, E–

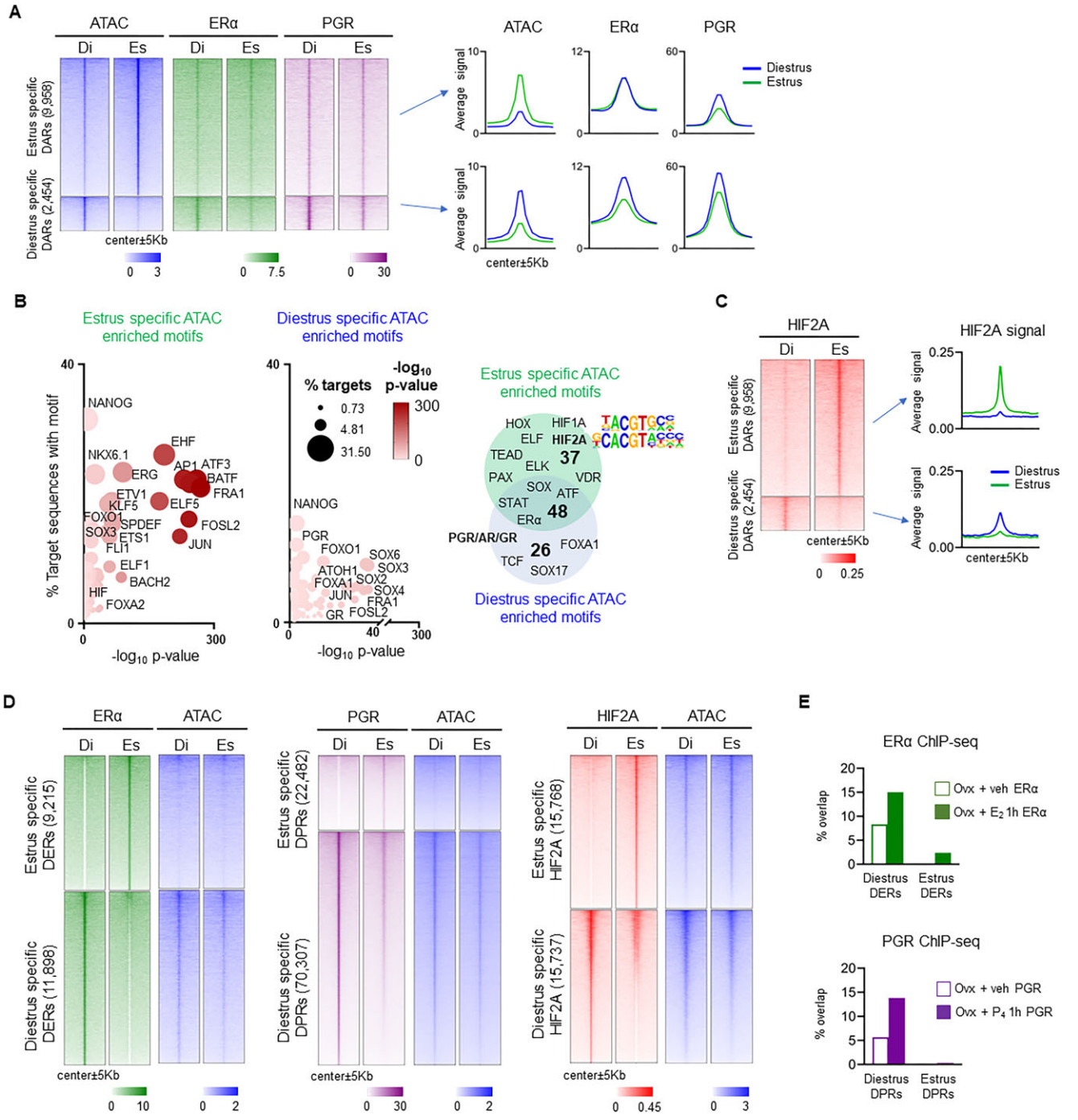

Figure 2. Estrous cycle dependent accessibility was characterized by distinct TF landscapes. (**A**) Heatmaps displaying ATAC-seq signal of differential ATAC-seq regions (DARs) ±2-fold between diestrus and estrus (loss and gain defined by estrus versus diestrus). ERα and PGR ChIP-seq signal is plotted in the same locations. Metaplots of diestrus and estrus average ATAC-seq signal, ERα and PGR ChIP-seq signal for estrus or diestrus specific DARs indicated by arrows. (**B**) Bubble plots of motif enrichment for diestrus and estrus specific DARs from Supplementary Table S3C and S3E, random group A. Size of bubble indicates number of times that motif was observed in estrus or diestrus specific DARs. Color scale indicates −log *P*-value. Select motifs are indicated. Venn diagram of motifs enriched in diestrus or estrus specific DARs (numbers of motifs and select motifs are indicated). (**C**) Heatmap of diestrus and estrus HIF2A ChIP-seq signal for diestrus and estrus specific DARs (plotted in the same order as panel A). Metaplots of diestrus and estrus HIF2A ChIP-seq signal at diestrus and estrus specific DARs indicated by arrows. (**D**) Heatmap of diestrus and estrus specific DERs (from Figure 1A), diestrus and estrus specific DPRs or diestrus and estrus specific differential HIF2A regions (DHRs) with ATAC-seq signal plotted in the same locations as the DERs, DPRs or DHRs. All heatmaps are organized from highest signal to lowest signal in estrus [ATAC in panel A; ERα, PGR and HIF2A in panel D (left to right, respectively)]. Heatmaps are plotted using the center of the peak ± 5 Kb. Intensity of ATAC-seq or ChIP-seq signal (reads mapped to each bin of 100 bp) is indicated by color intensity for each heatmap or on the y-axis of metaplots. (**E**) Graph of percent overlap between mouse estrus cycle specific DERs with ERα ChIP-seq peaks from ovx + vehicle or ovx + E_2 1 h (left). Graph of percent overlap between mouse estrus cycle specific DPRs with PGR ChIP-seq peaks from ovx + vehicle or ovx + P_4 1 h (right). ERα ChIP-seq data is from GSE36455 and PGR ChIP-seq data is from GSE34927 (6,30).

H). Estrus specific DER or DPR gain locations were observed in consistently closed chromatin regions (little to no ATAC-seq signal). In contrast, estrus specific HIF2A gain locations were found in regions of increased chromatin accessibility compared to diestrus. Diestrus specific ERα, PGR and HIF2A were observed in regions of accessible chromatin that became more closed during estrus. Taken together, these data suggest that chromatin accessibility during estrus is not governed by ERα or PGR but rather by other transcription factors, including HIF2A, while diestrus specific accessibility appears to coordinate with ERα and PGR binding.

To further explore the timing of receptor binding under the influence of either estrogen or progesterone, we overlapped DERs and DPRs with published ERα or PGR ChIP-seq peaks in ovx mice treated with 17β-estradiol or progesterone for 1 h compared to vehicle treatment (ERα ChIP-seq from GSE36455 and PGR ChIP-seq from GSE34927) (6,29). For ERα, there was 8.3% overlap of diestrus specific DERs with ERα in ovx mice in the absence of estrogen with increased overlap (15%) in the presence of estrogen (Figure 2E). In contrast, there was <3% overlap of either ovx group with estrus specific DERs. For PGR, there was a similar pattern of overlap with 5.7% overlap of diestrus specific DPRs with ovx mice in the absence of progesterone and increased overlap (13.8%) in the presence of progesterone (Figure 2E). There was very little overlap of estrus specific DPRs with either of the ovx groups. ERα and PGR binding in ovx mice in the presence of hormone overlaps ERα and PGR binding primarily during diestrus and not estrus, suggesting that the action of both hormones is most important during diestrus despite progesterone levels being higher in estrus (2). The overall low levels of overlap of ERα and PGR binding locations in intact cycling mice compared to ovx mice supports the idea that there is sufficient estradiol, progesterone, and likely other endocrine factors present at both stages of the estrous cycle to influence physiological ERα and PGR binding.

Chromatin accessibility is increased at promoter regions of genes up regulated during estrus

Estrous cycle dependent chromatin accessibility changes suggested that these changes could regulate expression of nearby genes. There were 2060 differentially expressed genes (DEGs) increased in estrus and 2101 DEGs decreased in estrus relative to diestrus (Figure 3A; Supplementary Table S4). To determine if chromatin accessibility changes at gene promoters correlated with the direction of gene expression changes, we subtracted ATAC-seq signal in diestrus from that in estrus at the TSS ± 1 kb. Of the 2060 up-regulated DEGs (estrus to diestrus), 1458 (70.8%) had increased ATAC-seq signal while only 523 (25.4%) had decreased signal (Figure 3B and Supplementary Table S5A). Of the 2101 down-regulated genes, 1335 (63.5%) had decreased ATAC-seq signal while only 635 (30.2%) had increased ATAC-seq signal (Figure 3B and Supplementary Table S5B). A close examination of these data revealed large changes in ATAC-seq signal from diestrus to estrus in a subset of up-regulated genes. Violin plots of ATAC-seq signal were generated with the up-regulated genes split into two categories: ATAC-seq ≥2-fold (109 DEGs) or <2-fold (1951 DEGs) (Figure 3B and Supplementary Table S5C, D). As expected, there was a robust significant increase in accessibility at the promoter region of genes with the highest fold change in ATAC-seq signal (Figure 3B and Supplementary Table S5C). Interestingly, these genes had very low ATAC-seq signal during diestrus, suggesting they exhibited closed chromatin that was opened during estrus. The remaining up-regulated DEGs (ATAC-seq <2-fold change) had significantly higher ATAC-seq signal in diestrus than the ≥ 2-fold change group but this was also significantly increased in estrus (Figure 3B and Supplementary Table S5D). There were only 14 down-regulated DEGs that had a ≥2-fold change in ATAC-seq signal, so this group was not split. There was much lower ATAC-seq signal at the TSS of these genes compared to the up-regulated genes (ATAC-seq <2-fold) and there was no significant difference between diestrus and estrus in this group (Figure 3B and Supplementary Table S5E). These findings point at alterations in promoter chromatin accessibility as a likely contributor to gene expression changes only in genes up regulated during estrus.

ERα binding at the promoters of estrous cycle dependent genes is static while PGR binding is lost from diestrus to estrus

To determine if ERα or PGR binding influenced gene expression changes and/or chromatin accessibility at the promoters of DEGs (TSS ± 1 kb), metaplots of ERα and PGR ChIP-seq signal were generated; ATAC-seq signal is included for reference (Figure 3C). The 109 up-regulated DEGs that had ≥2-fold increased ATAC-seq signal at promoters had increased ERα and HIF2A during estrus compared to diestrus but low unchanging levels of PGR. In contrast, the remaining DEGs (up- and down-regulated) with lower ATAC-seq signal changes had no change in ERα between groups and minimally decreased PGR in estrus compared to diestrus. There was an increase in HIF2A during diestrus compared to estrus at both up- and down-regulated DEGs. These data indicate that ERα and PGR binding is relatively static at the TSS of most DEGs across the estrous cycle and does not appear to influence gene expression. However, a small subset of up-regulated DEGs have increased accessibility where ERα is coordinately increased and no change in PGR binding, suggesting direct estrogen regulation at accessible chromatin of these few genes. The TSS of these genes also had increased HIF2A binding, suggesting a role for this transcription factor in gene expression regulation.

Dynamic enhancers near estrous cycle dependent genes exhibit two modes of action

To examine chromatin accessibility changes at presumed enhancers near DEGs, we restricted the ≥2-fold change DARs to ±100 kb of a DEG (excluding the promoter; TSS ± 5 kb); these restricted DARs near DEGs were designated 'dynamic enhancers'. We defined regions where DARs had increased open chromatin at diestrus as 'diestrus specific' and regions where DARs had increased open chromatin at estrus as 'estrus specific'. Of the 2727 dynamic enhancers, only 439 (16%) were diestrus specific considering both up- and down-regulated genes (Figure 3D and Supplementary Table S6A, B). Regardless of the direction in gene expression changes, these diestrus specific enhancers had coordinate diestrus specific ERα and PGR binding that was lost during estrus; HIF2A followed the same pattern as ERα and PGR. Most of the dynamic enhancers were estrus specific and were found near estrus specific up-regulated DEGs (1783; 65%); fewer were near down-

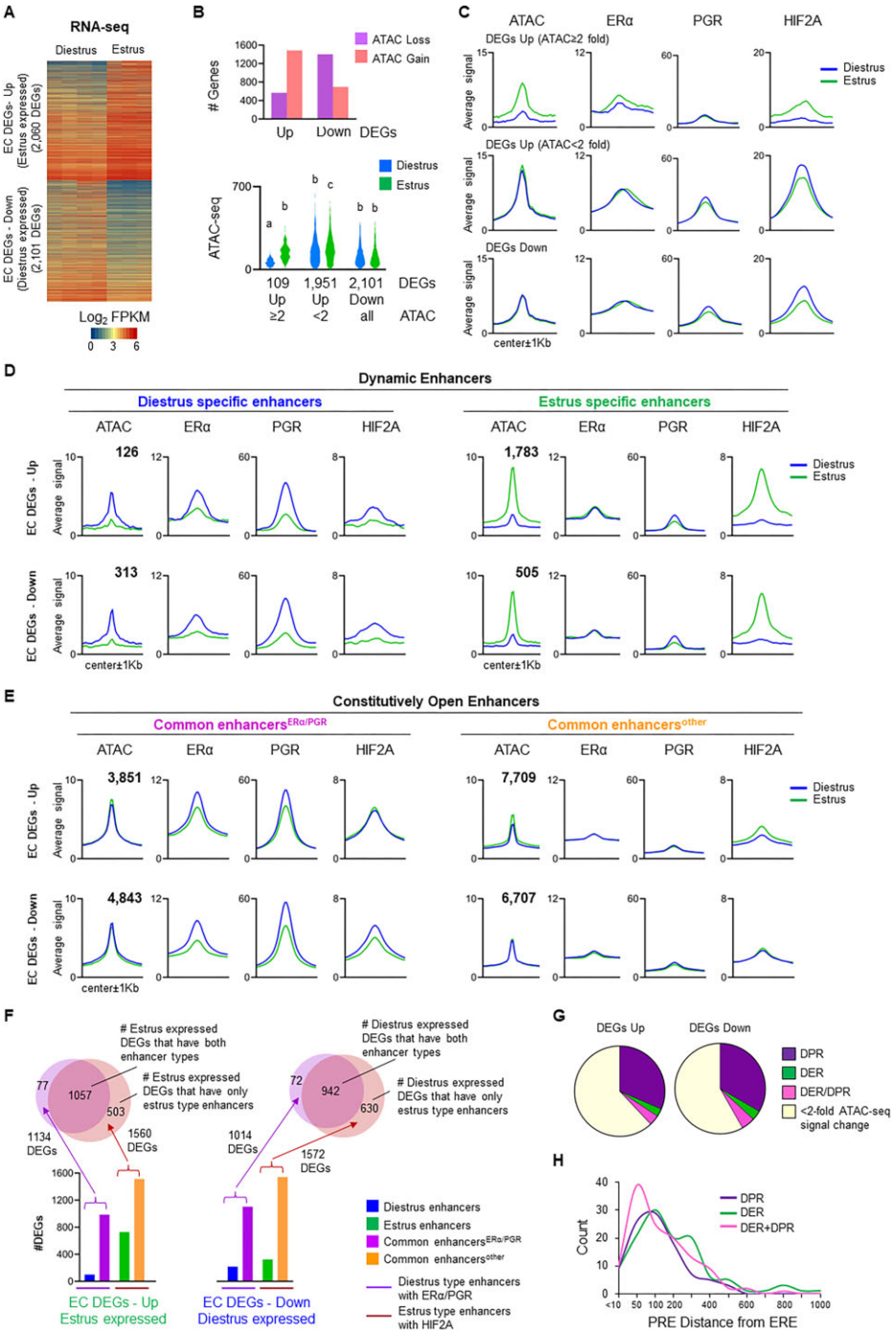

Figure 3. ERα and PGR were bound together during diestrus at dynamic and constitutively open enhancers near estrous cycle dependent genes. (**A**) Heatmap of estrous cycle (EC) differentially expressed genes (DEGs) of estrus versus diestrus (cutoffs of FPKM > 1.0, FDR ≤ 0.05 and ≥1.5-fold change). Log_2 transformed FPKM values are shown split by EC DEGs – up (estrus expressed) and EC DEGs – down (diestrus expressed); number of DEGs is indicated (diestrus, $n = 4$; estrus, $n = 3$). (**B**) Graph of the number of EC DEGs up- and down-regulated with average ATAC-seq signal gain or loss (estrus versus diestrus) at the TSS ± 5 kb; genes with no ATAC-seq change in average signal at the TSS are not included. Violin plots of average ATAC-seq signal at the TSS ± 5 kb of EC up-regulated DEGs is split into ATAC-seq signal ≥2-fold change and <2-fold change and EC down-regulated DEGs. Each letter represents significant difference from other groups ($P < 0.05$ using one-way ANOVA followed by Tukey's test). Number of genes in each category is indicated. (**C**) Metaplots of diestrus and estrus ATAC-seq, ERα, PGR and HIF2A ChIP-seq signal at the TSS of EC DEGs split into the same three categories in panel B. Data was plotted with the TSS at the center ±1 kb. Intensity of ATAC-seq or ChIP-seq signal (reads mapped to each bin of 100bp) is indicated on the y-axis of metaplots. (D, E) Metaplots of DARs ± 100 kb of the TSS of EC DEGs excluding the TSS ± 5 kb (dynamic enhancers) split into diestrus or estrus specific (**D**) or constitutively open enhancers (ATAC-seq signal that is not changing between estrus and diestrus) further split into those overlapped with either ERα or PGR (common enhancers$^{ERα/PGR}$) or lacking ERα or PGR (common enhancers^{other}) (**E**); signal during diestrus and estrus is shown for each metaplot. ERα, PGR and HIF2A ChIP-seq signal is also plotted for the same locations. The number of regions is indicated in bold for each group. (**F**) Graph of the number of EC DEGs in each of the enhancer categories from panels D and E. Venn diagrams of DEGs from diestrus type enhancers (diestrus specific and common$^{ERα/PGR}$) were overlapped with DEGs from estrus type enhancers (estrus specific and common^{other}) split by up- and down-regulated genes. Number of DEGs is indicated. (**G**) Pie charts of overlap of DPRs, DERs, both or neither in constitutively open enhancer regions that overlap ERα or PGR. (**H**) Graph of the distance between EREs and PREs at DPRs, DERs or both at common enhancers in panel E.

regulated DEGs (505; 19%) (Figure 3D and Supplementary Table S6C, D). For estrus specific dynamic enhancer regions, there was low ERα and PGR ChIP-seq signal compared to diestrus specific regions (Figure 3D). There were only minor reductions in PGR signal in estrus compared to diestrus in these regions, and ERα did not change, regardless of whether the genes were up- or down-regulated. In contrast, HIF2A was highly associated at these enhancers during estrus and this association was lost during diestrus. These data, combined with motif analysis of DARs, suggest that diestrus specific enhancers are under direct regulatory control of ERα and PGR while estrus specific enhancers are most likely under the influence of other transcription factors such as HIF2A.

Most enhancers near estrous cycle dependent DEGs are constitutively open and many are highly occupied by ERα and PGR during diestrus

In addition to dynamic enhancers, constitutively open chromatin regions can also impact nearby gene expression through changes in transcription factor (TF) association (37). We identified constitutively open enhancer regions, which we refer to as 'common enhancers', as all regions that had ATAC-seq peaks but were not DARs and were near DEGs (±100 kb of the TSS but excluding the TSS ± 5 kb). This resulted in 11 560 common enhancers near upregulated DEGs and 11 550 common enhancers near downregulated DEGs (Supplementary Table S7A, B). To focus on estrous cycle changes in ERα and PGR binding at common enhancers, we first restricted our analysis to those with either ERα or PGR ChIP-seq peaks overlapped in those locations (common enhancers$^{ER\alpha/PGR}$); there were 3851 near upregulated DEGs and 4843 near downregulated DEGs (Figure 3E and Supplementary Tables S7C-D). There were three times as many common enhancers$^{ER\alpha/PGR}$ compared to dynamic (8694 versus 2727) with 44% near up-regulated genes and 56% near down-regulated genes. These common enhancers$^{ER\alpha/PGR}$ had much higher levels of ERα and PGR than at dynamic enhancers (Figure 3D, E). Like diestrus specific dynamic enhancers, both ERα and PGR were lost from common enhancers$^{ER\alpha/PGR}$ during estrus, regardless of the change in direction of gene expression. Diestrus specific HIF2A was also observed at these common enhancers$^{ER\alpha/PGR}$ but unlike ERα and PGR, HIF2A was only lost during estrus when the enhancer was near down-regulated DEGs, suggesting a more complex pattern of binding for this transcription factor.

The remaining common enhancers that did not have ERα or PGR overlapped (common enhancers^{other}) were evaluated for potential changes in HIF2A; there were 7709 near up regulated DEGs and 6707 near down regulated DEGs (Figure 3E and Supplementary Table S7E-F). Metaplots of ATAC-seq, ERα and PGR confirmed that these locations were constitutively open and generally lacked ERα and PGR. The ATAC-seq signal was much lower (∼25–35% lower ATAC-seq signal at the peak) for this set of common enhancers^{other} compared to the common enhancers$^{ER\alpha/PGR}$; ATAC-seq signal was also ∼35% lower than estrus specific enhancers during estrus. HIF2A was increased during estrus compared to diestrus but only when near up-regulated DEGs, suggesting a role for HIF2A in this group of genes. This association correlated with some increase in accessibility and resembled the patterns observed for estrus specific enhancers. A summary of the number of genes near each type of enhancer showed that estrus specific enhancers were preferentially near upregulated DEGs (730 of 2060; 35%) instead of downregulated DEGs (323 of 2101; 15%) (Figure 3F). Common enhancers$^{ER\alpha/PGR}$ were found in similar numbers near up-regulated genes (986 of 2060; 48%) and down-regulated DEGs (1105 of 2101; 53%). Common enhancers^{other} were found near ∼75% of both up- and down-regulated DEGs. This group, however, had some of the lowest ATAC-seq signal of the enhancer groups, suggesting they do not influence gene expression as much as the other enhancer types.

The observed TF binding patterns generally separate into two categories of enhancers, those that had diestrus specific ERα/PGR binding (diestrus type enhancers) or those that lack ERα/PGR but instead had estrus specific HIF2A binding (estrus type enhancers). To investigate if DEGs had one or both of these two different types of enhancers, we first identified the genes that had a diestrus type enhancer (diestrus specific or common enhancers$^{ER\alpha/PGR}$) and the genes that had an estrus type enhancer (estrus specific or common enhancers^{other}). There were 1134 DEGs up and 1014 DEGs down that had a diestrus type enhancer and 1560 DEGs up and 1572 DEGs down that had an estrus type enhancer. Overlaps of these DEGs showed almost all up- and down-regulated DEGs that had a diestrus type enhancer also had an estrus type enhancer suggesting switching between the two enhancer types during the estrus cycle. In contrast, there were some DEGs that only had estrus type enhancers; 503 DEGs up and 630 DEGs down. These data suggest that these genes rely either on promoter TF occupancy of ERα/PGR or enhancers occupied by HIF2A and not nearby ERα/PGR.

To further assess this coordinated loss of both receptors in the common enhancers$^{ER\alpha/PGR}$, an overlap of DERs and DPRs with these regions was performed. More than half of the common enhancers$^{ER\alpha/PGR}$ exhibited little to no change (<2-fold) in ERα or PGR near both up- and downregulated genes (Figure 3G). However, primarily from diestrus to estrus, 35–38% lost PGR, 7–8% lost ERα, and 4–5% lost both. An analysis of distance of the PGR response element (PRE) and the ERE in the common enhancer locations that had a DER, DPR or both revealed that the two receptors bound in close proximity when lost together during estrus and bound further apart when only one or the other was lost during estrus (Figure 3H). These data suggest that the proximity of ERα and PGR binding elements to each other appears to influence binding of both receptors together at constitutively open chromatin during diestrus, and association of both receptors in these locations is lost during estrus.

Estrogen is the main driver of estrous cycle dependent gene expression

Estrogen and progesterone are thought to be the main drivers of uterine estrous cycle gene expression changes. To determine which genes were directly influenced by estrogen or progesterone, we overlapped estrous cycle dependent DEGs with uterine gene expression from ovx mice that were exposed to either estradiol alone or progesterone alone (38,39). Of the 2060 genes increased during estrus, 1463 (71%) were also increased 2 h and/or 24 h after estradiol treatment [data from (38); GSE53812] (Figures 4A and Supplementary Figure S7A, B) (38). Top GO categories of these genes were related to cell proliferation activities: cell division/cycle, kinase activity, biosynthetic processes, and oxidoreductase (Figure 4B

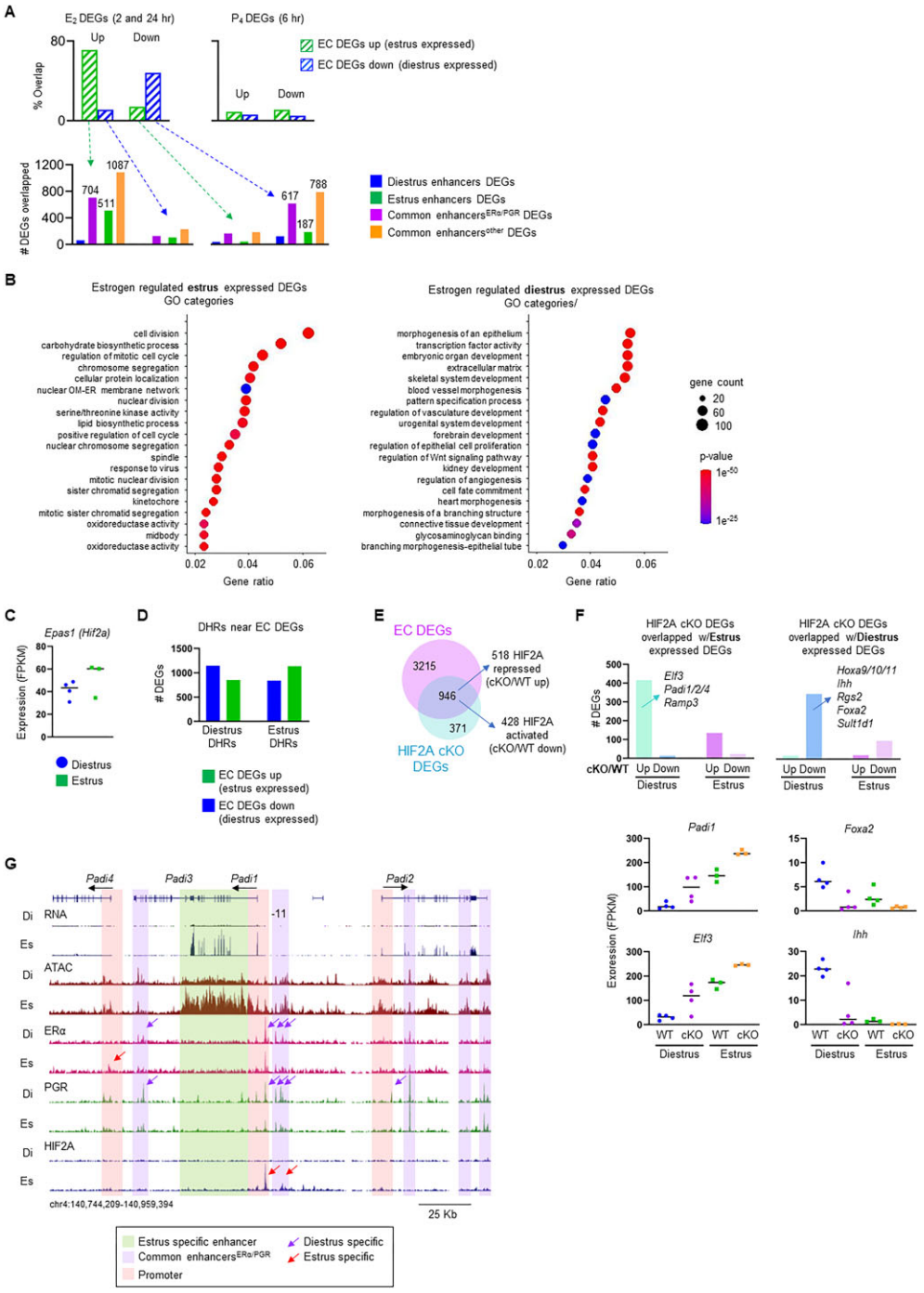

Figure 4. Estrogen is the main driver of EC dependent gene expression; HIF2A also plays a role. (**A**) Graph of the percent overlap of EC up- or down-regulated DEGs with estradiol (E_2) regulated DEGs in ovx mice (up- or down-regulated, E_2 2 h + 24 h/veh; data from Winuthayanon *et al.*, 2014; GSE53812) or progesterone (P_4) regulated DEGs in ovx mice (up- or down-regulated, P_4 6h/veh); data from Kommagani *et al.*, 2014; GSE31406) (39,40). Graph of estrogen regulated EC DEGs (upregulated, left; downregulated, right) overlapped with each enhancer category from Figure 3D, E. Arrows indicate groups. (**B**) Pathway analysis of EC up-regulated DEGs that are up-regulated by estrogen (top) and EC down-regulated DEGs that are down-regulated by estrogen (bottom). Top 20 GO categories as determined by *P*-value are plotted by gene ratio (#genes in GO category/#DEGs in that group); *P*-value indicated by color and #genes indicated by size (taken from Supplementary Table S7A, B). (**C**) Graph of *Hif2a* mRNA expression during diestrus and estrus plotted as FPKM from RNA-seq data. Each point represents an individual sample. (**D**) Graph of the number of EC DEGs up- or downregulated that have a diestrus or estrus specific DHR ± 100 kb of the TSS of EC DEGs. (**E**) Venn diagram of all EC DEGs overlapped with all HIF2A cKO versus wild type (WT) DEGs (cutoffs of FPKM > 1.0, FDR ≤ 0.05 and ≥1.5-fold change). Of the overlapped group, the number of up- and downregulated are indicated. (**F**) Graph of the number of EC DEGs split into up- and downregulated (estrus expressed and diestrus expressed, respectively) that were overlapped with HIF2A cKO versus WT DEGs split into up- or down-regulated during diestrus or estrus. Select genes are in specific groups are indicated. Graphs of mRNA expression (FPKM) of representative genes in two of those groups; *Padi1*, *Elf3*, *Foxa2* and *Ihh* ($n = 3$-4 per group). (**G**) UCSC genome browser tracks of the *Padi* gene family locus. Tracks are RNA-seq, ATAC-seq, ERα, PGR and HIF2A ChIP-seq signal in diestrus and estrus samples; Refseq genes are indicated above the tracks and genomic location and size are indicated under the tracks. Color shading indicates the type of enhancer and the promoter regions (~TSS ± 5 kb). Purple arrow indicates diestrus specific signal and red arrow indicates estrus specific signal.

and Supplementary Table S8A). In addition, ∼50% (1005 of 2101) of the genes that were highly expressed during diestrus and reduced during estrus were decreased with estradiol treatment. Top GO categories for this group of genes were related to tissue morphogenesis: morphogenesis, extracellular matrix (ECM), Wnt signaling and vasculature (Figure 4B and Supplementary Table S8B). These data show that two different types of cellular processes occur under the influence of estrogen during these two phases of the estrous cycle. Additionally, the majority of estrous cycle DEGs that overlapped estradiol DEGs (>80%) were either expressed 24 h later or both 2 h and 24 h later (sustained expression over time) as opposed to only 2 h (early gene expression) suggesting the observed estrous cycle gene expression changes were observed ∼24 h after initiating events. Therefore, ERα/PGR binding during diestrus most likely impacted transcription levels observed during estrus (∼24 h later) (Supplementary Figure S7B).

In contrast, estrous cycle dependent gene expression changes were not highly overlapped with progesterone regulated gene expression (≤11% in either direction) (data from Kommagani *et al.*, 2014; GSE31406) (Figures 4A and S7A, B) (39). These data suggest that a large portion of estrous cycle dependent gene expression changes can be attributed to increasing estrogen levels that occur during diestrus to proestrus that result in gene expression changes 24–36 h later during estrus. Progesterone exposure alone in the ovx mouse model does not recapitulate estrous cycle gene expression changes, suggesting estrogen is required for most progesterone influenced gene expression in the uterus of intact cycling mice.

To assess the influence of estrogen on enhancers near estrous cycle DEGs, we determined how many of the estrous cycle DEGs were near each of the enhancer types that were also regulated by estradiol (Figure 4A). Estrus specific enhancers were predominantly found near estrous cycle DEGs that were highly expressed during estrus and upregulated by estradiol in the ovx model, despite the lack of ERα binding in these locations. Common enhancers^{other} were also found preferentially near estrogen regulated DEGs that were highly expressed during estrus, suggesting a similar mode of action as the estrus specific enhancers. Common enhancers$^{ERα/PGR}$ were found equally associated with estrous cycle dependent DEGs that were upregulated by estradiol and highly expressed during estrus as well as downregulated by estradiol and highly expressed during diestrus (Figure 4A). These locations were occupied by both ERα and PGR during diestrus and both were lost during estrus (Figure 3E), suggesting direct control of gene expression by ERα during diestrus with potential influence of PGR.

HIF2A directs gene expression toward diestrus expression patterns

The accumulation of HIF2A at estrus specific enhancers suggested a role for this protein in estrus cycle dependent gene expression. *Hif2a* (also known as *Epas1*) was not among the estrus cycle DEGs and its expression appeared to be stable across the estrous cycle (Figure 4C). To determine if HIF2A could influence gene expression, we used the differential HIF2A ChIP-seq binding locations and restricted them to ± 100 kb of estrous cycle DEGs (Figure 4D and Supplementary Tables S1E, F). There were > 1000 diestrus expressed DEGs with a diestrus specific HIF2A binding site nearby and >1000 estrus expressed DEGs that had an estrus specific HIF2A binding site nearby. To determine if HIF2A actually influenced estrus cycle dependent gene expression, we generated a uterine conditional HIF2A knock out mouse. *Hif2a* (*Epas1*) floxed mice were crossed with PGR-cre mice (*Epas1* flox/flox, PGR-cre+; HIF2A cKO) and RNA-seq was performed during diestrus and estrus. A comparison of HIF2A cKO to wild type (*Epas1* flox/flox; WT) mice revealed 1062 DEGs at diestrus and 405 DEGs at estrus (Supplementary Table S9A, B). An overlap of these DEGs with estrus cycle DEGs resulted in 946 in common; 518 upregulated and 428 downregulated (Figure 4E). To further explore how HIF2A influenced gene expression during diestrus and estrus, DEGs were split into diestrus expressed (highest during diestrus) or estrus expressed (highest during estrus) and then overlapped with HIF2A cKO versus WT DEGs (Figure 4F). The highest overlap was in estrus expressed genes that were upregulated upon loss of HIF2A, suggesting a major role of HIF2A in repressing these genes; examples included many estrogen regulated genes such as *Padi1/2/4*, *Elf3* and *Ramp3* (38) (Figure 4F). The second most overlapped group was estrus expressed genes that were downregulated in the HIF2A cKO. Examples in this category included genes highly expressed in glandular epithelium such as *Foxa2, Spink1, Gpx3* and *Sult1d1* as well as genes involved in female reproductive tract development and function, including *Hoxa9/10/11* and *Ihh* (18,40,41). Gene expression patterns from both groups show that lack of HIF2A drives gene expression towards estrus expression patterns and, therefore, that HIF2A drives gene expression toward diestrus expression patterns (Figure 4F). These data, combined with evidence for HIF2A binding at promoters and estrus specific enhancers, show that this protein is a direct mediator of specific estrous cycle gene expression changes.

Examples of some of the most highly differentially regulated genes were the peptidyl arginine deiminases, *Padi1*, *Padi2* and *Padi4* (upregulated in estrus compared to diestrus 21.7-, 18.3- and 12.2-fold, respectively); *Padi3* was only minimally expressed in the uterus (Supplementary Table S4). This estrus specific increase in mRNA expression was accompanied by some of the highest ATAC-seq signal at the promoters of these genes during estrus. The *Padi* genes are all found in a single gene locus on chromosome 4 (Figure 4G). *Padi1* is among the 109 up-regulated DEGs that have ≥2-fold ATAC-seq signal at the TSS (Figure 3B-C and Supplementary Table S5C). In addition to the 2-fold increased ATAC-seq signal at the promoter during estrus compared to diestrus, both ERα and PGR are associated during diestrus and only moderately reduced during estrus (Figure 4D). There was also a substantial increase in HIF2A signal near the TSS during estrus compared to diestrus. *Padi1* was upregulated in the absence of HIF2A, confirming a repressive role for HIF2A in controlling *Padi1* gene expression (Supplementary Table S9A, B). ATAC-seq signal was increased at *Padi2* and *Padi4* promoters (1.83-fold and 1.99-fold, respectively; estrus versus diestrus) suggesting a similar mechanism of action as *Padi1* (Supplementary Table S5D). HIF2A was minimally associated at the *Padi2* and *Padi4* TSS but HIF2A cKO mice showed increased expression of *Padi2* and *Padi4* over WT controls similar to *Padi1*, suggesting HIF2A binding at the *Padi1* TSS may influence the entire *Padi* locus. There was a common enhancer$^{ERα/PGR}$ ∼11 kb upstream of *Padi1* that had both ERα and PGR binding during diestrus that was lost during estrus and HIF2A binding that was estrus specific, suggesting a shift in TF control in this region; we

have previously shown looping of this region to the promoter during uterine development (Figure 4G and Supplementary Table S7C) (42). There was also a highly dynamic region in the gene body of *Padi1* with excessive accumulation of ATAC-seq signal during estrus that was lost during diestrus. This region was largely unoccupied by ERα or PGR, suggesting that accessibility and not direct hormone receptor binding plays a predominant role in the large fold changes in expression of this gene. There were common enhancers$^{ERα/PGR}$ near *Padi2* and *Padi4* that had a range of ERα and PGR occupancy, suggesting more complexity of gene expression control for these two genes compared to *Padi1* (Figure 4D and Supplementary Tables S7C and S7E). We interpret these findings to indicate that some of the most highly expressed genes during estrus are highly stimulated by ERα/PGR binding during diestrus, providing sustained transcriptional output that peaks during estrus. ERα/PGR binding is then lost during estrus and replaced by indirect targets of ERα/PGR signaling such as HIF2A to repress expression to lower levels during diestrus.

Proteins in complex with ERα are estrous cycle dependent

The differences in ERα binding locations over the estrous cycle along with enrichment in distinct TF motifs suggested that there were estrous cycle stage-dependent differences in direct ERα binding partners. To test this idea, we performed Rapid Immunoprecipitation Mass spectrometry of Endogenous proteins (RIME) to identify the proteins directly bound to ERα in diestrus and estrus uteri (Supplementary Tables S8A, B). Comparison of diestrus to estrus ERα binding partners revealed substantial differences (Figures 5A and Supplementary Figure S8; Supplementary Tables S10A, B). There were 89 proteins in common including the histone deacetylases, HDAC1 and HDAC2; HDAC1 was shown previously to bind ERα (43). Another protein in this group was PRMT1, a protein that methylates ERα in the DNA binding domain to trigger extranuclear activity (44). Several proteins were associated with ERα in both diestrus and estrus but had a much higher rate of observation (spectral count) in one stage compared to the other (Figure 5A). For example, HDAC1 was observed more often with ERα during estrus while CHD4 was more often captured with ERα during diestrus. CHD4 is a chromatin modifier and a member of the NuRD complex that is found at enhancers; its activity can impact chromatin accessibility by interacting with HDACs (45).

There were 23 proteins associated with ERα during estrus but not diestrus, including PADI2 (Figure 5A and Supplementary Table S10A, B). Identification of PADI2 as an estrus specific ERα binding protein supports previous findings that PADI2 facilitates ERα binding by citrullinating histone H3R26 at ERα binding sites and confirms these two proteins are actually in complex together (46,47). Sixty proteins were associated with ERα during diestrus but not estrus; some of these have been previously reported as ERα binding partners such as STAT3, calmodulin (CALM) and PGR (48–50) (Figures 5A and Supplementary Figure S8, Supplementary Table S10A, B). The presence of PGR in complex with ERα only during diestrus supports the ChIP-seq data presented herein where ERα and PGR are bound to chromatin together during diestrus. Two cohesin complex proteins, SMC1A and SMC3, were diestrus specific, suggesting a hormone dependent role in ERα binding to looped chromatin. In agreement, ERE motifs are highly enriched at SMC1A binding sites in the uterus of ovx mice (51). Taken together, this robust differential protein association due to estrous cycle stage confirms the dynamic changes in ERα binding partners and may explain some of the differential transcription factor landscape of ERα binding to DNA.

3D chromatin architecture is impacted by the estrous cycle

The differential association of ERα with the cohesin complex proteins, SMC1A and SMC3, during diestrus suggested a potential impact on chromatin architecture. SMC1A is found at the contact points of looped chromatin (52). An overlap of published uterine SMC1A ChIP-seq peaks in ovx mice with the DERs identified in this study showed more than twice as many overlapping regions in diestrus as estrus (data from Hewitt *et al.*, 2020; GSE147843) (Figure 5B) (51). In addition, SMC1A ChIP-seq peaks were highly overlapped with regions that have both DERs and DPRs found together compared to regions that had only one of the two (Figure 5B). These data support the preferential association of SMC1A with ERα during diestrus and suggests locations that have both receptors are more likely to be functionally looped. To identify changes in chromatin architecture over the estrous cycle, we performed HiC-seq on diestrus and estrus samples. Interaction matrices for diestrus and estrus samples showed the expected robust looping within chromosomes (Supplementary Figure S9A). There were twice as many diestrus specific DERs overlapped with HiC-seq loop ends as estrus specific DERs, confirming the preferential association of ERα at loop ends during diestrus (Figure 5C).

To further examine the impact of the estrous cycle on 3D chromatin structure, loops were identified at both diestrus and estrus and then these regions were overlapped. There were >28 000 chromatin loops observed in both diestrus and estrus uterine samples; 14 202 of these loops overlapped and were likely stable (Figure 5D; Supplementary Table S11A, B). There were 16 270 diestrus specific loops and 14 001 estrus specific loops, indicating substantial estrous cycle dependent chromatin rearrangement. For diestrus specific loops, diestrus specific ERα was overlapped more than twice as often as estrus specific ERα; PGR showed a similar pattern (Figure 5D). HIF2A was also observed at diestrus specific loops, with less estrous cycle dependence than either ERα or PGR. Interestingly, estrus specific loops also overlapped diestrus specific ERα and PGR more often than estrus specific ERα and PGR, but the overall total number of locations were fewer than diestrus specific loops (Figure 5D). This was not the case for HIF2A as there was slightly more estrus specific HIF2A than diestrus specific HIF2A associated with estrus specific loops. HiC-seq loops that were found in common between diestrus and estrus also had preferential overlaps with diestrus specific ERα and PGR while HIF2A was less estrous cycle dependent (Figure 5D). Taken together, ERα and PGR binding were highly associated with chromatin loops that formed during diestrus but were lost during estrus, confirming the diestrus specific association of ERα and cohesin proteins observed by RIME.

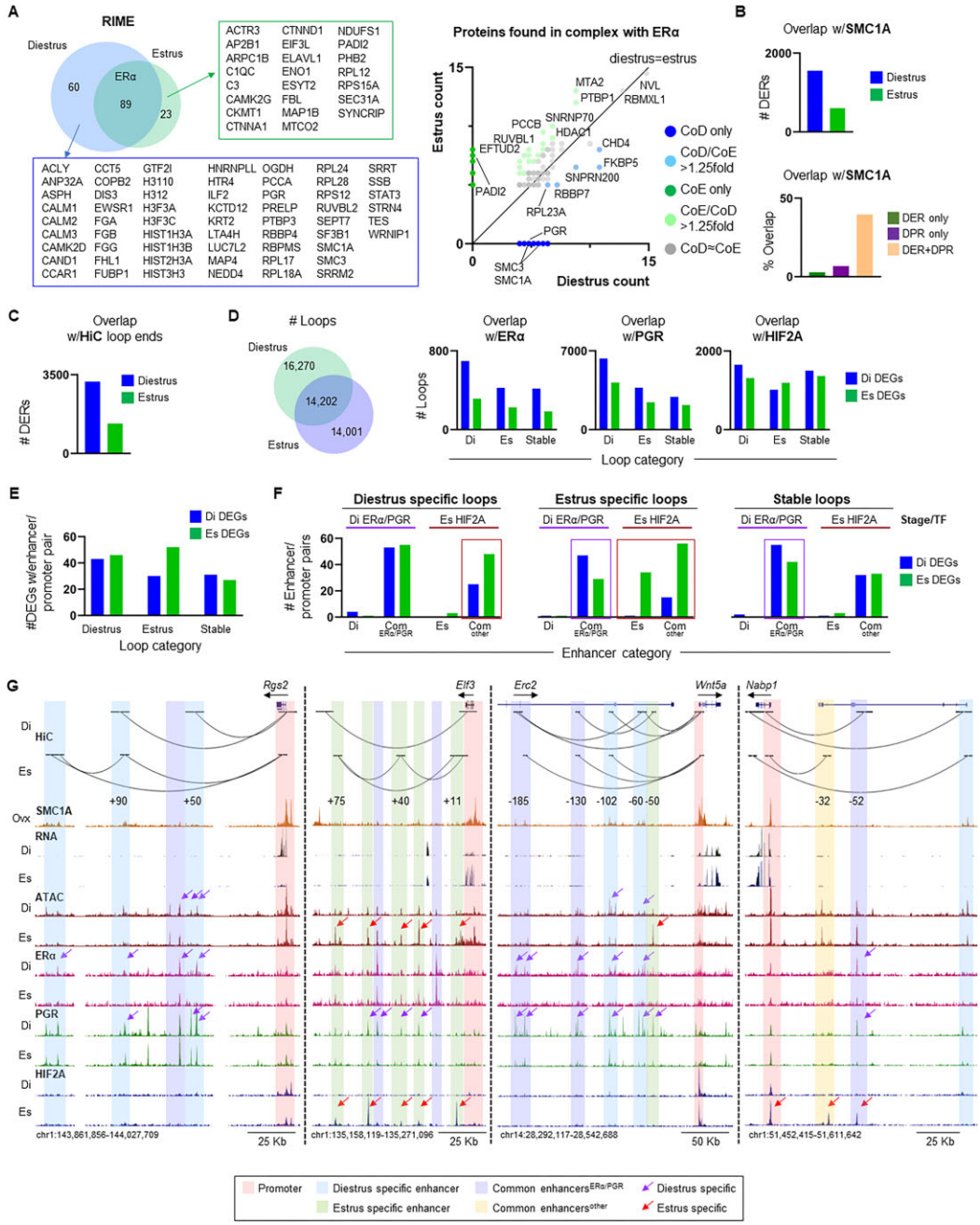

Figure 5. ERα binding partners and chromatin structure change with estrous cycle stage. (**A**) Venn diagram of proteins bound to ERα in diestrus and estrus; non-overlapped proteins are listed (diestrus, blue box; estrus, green box). Graph of spectral counts (number of times that peptide was observed) for diestrus and estrus (normalized to reflect differences in ERα pull down in diestrus versus estrus). Line plotted is slope = 1 where diestrus counts = estrus counts. Diestrus specific proteins are in blue, estrus specific proteins are in green, proteins that were 1.25-fold increased (diestrus/estrus) are in light blue and 1.25-fold increased (estrus/diestrus) are in light green; proteins with <1.25-fold difference are in gray. Select proteins are indicated. (**B**) Graph of the number of diestrus and estrus specific DERs that are overlapped with uterine SMC1A ChIP-seq peaks in ovx mice (data from GSE147843) (45). Graph of the percent overlap of SMC1A ChIP-seq peaks and DERs, DPRs or locations that have both receptors (DER + DPR). (**C**) Graph of number of diestrus and estrus specific DERs that overlap HiC-seq loop ends observed in diestrus and estrus. (**D**) Venn diagram of HiC-seq loops observed in diestrus and estrus; number of loops indicated. Graphs of the number of HiC-seq loops (split into diestrus specific, estrus specific and stable loops) overlapped with ERα, PGR or HIF2A peaks in diestrus and estrus. (**E**) Graph of the number of EC DEGs split into up- and downregulated with at least one enhancer/promoter pair split into diestrus specific loops, estrus specific loops and stable loops. (**F**) Graphs of the number of enhancer/promoter pairs from diestrus specific loops (left), estrus specific loops (middle) and stable loops (right) split into enhancer categories from Figure 3D-E. The occupancy of TFs (ERα/PGR or HIF2A) and the stage of occupancy is indicated across the top of each graph. Red boxes indicate loops that have preferential enhancer/promoter pairs of estrus expressed DEGs; note estrus specific enhancer/promoter pairs with estrus specific loops are entirely associated with estrus expressed DEGs. Purple boxes indicate loops that have preferential enhancer/promoter pairs of diestrus expressed DEGs. (**G**) Browser tracks of *Rgs2* locus, *Elf3* locus, *Wnt5a* locus and *Nabp1* locus. Tracks are HiC-seq loops, RNA-seq, ovx SMC1A ChIP-seq from Hewitt *et al.*, 2020 (52), ATAC-seq, ERα, PGR and HIF2A ChIP-seq signal in diestrus and estrus samples; Ref-seq genes indicated at top and genomic location and size indicated at bottom. Approximate distance of loop ends to the TSS of each gene is indicated (negative numbers are upstream and positive numbers are downstream). Color shading indicates the type of enhancer at loop ends and the promoter regions (~TSS ± 5 kb). Purple arrow indicates diestrus specific signal and red arrow indicates estrus specific signal.

Chromatin rearrangement at enhancer/promoter pairs of estrous cycle dependent DEGs

To determine if estrus cycle specific changes in chromatin looping were associated with DEGs, enhancer/promoter pairs at DEGs were identified (HiC loops that connect an enhancer, as defined by accessibility in Figure 3D, E, to a promoter of a DEG) (Supplementary Table S12). Typically, active enhancer/promoter pairs are defined by the presence of histone H3K27ac; however, H3K27ac is dispensable for enhancer activity at accessible chromatin regions and acetylation of residues other than lysine 27 of both H3 and H4 can indicate activity (53,54). For these reasons, we assumed accessibility combined with looping to the promoter could impact transcription and used the more inclusive definition of chromatin accessibility for enhancer/promoter pair identification. There were 203 DEGs that had a least one enhancer/promoter pair identified within 100 kb of the TSS (∼5% of DEGs) (Supplementary Table S12). Diestrus specific loops with enhancer/promoter pairs were found at 89 DEGs (46 up and 43 down) (Figure 5E). The enhancer/promoter pairs in these loops were predominantly common enhancers$^{ER\alpha/PGR}$ near both up- and down-regulated DEGs, demonstrating that loops formed during diestrus can be involved in activation or repression of gene expression and have ERα/PGR binding during loop formation (Figure 5F). Diestrus specific loops with common enhancers^{other} were preferentially found near genes that were repressed during diestrus and expressed during estrus; HIF2A was found in these locations. Estrus specific loops with enhancer/promoter pairs were preferentially found near genes highly expressed during estrus (82 DEGs; 52 up and 30 down) (Figure 5E). Enhancer/promoter pairs found at estrus specific loops were highly overlapped with both estrus specific enhancers (only near estrus expressed genes) and common enhancers^{other} predominantly near genes highly expressed during estrus; HIF2A was found in these locations and acts to down regulate gene expression observed during diestrus (Figures 4F and 5F). Estrus specific loops were also found at common enhancers$^{ER\alpha/PGR}$ that were preferentially at genes highly expressed during diestrus (downregulated DEGs) suggesting repression of gene expression during estrus that was alleviated during diestrus and allowed gene expression. Stable loops with enhancer/promoter pairs were found near the fewest number of DEGs with no overall estrus cycle dependent gene expression preference (58 DEGs; 27 up and 31 down) (Figure 5E). Enhancer/promoter pairs found at stable loops most often involved common enhancers$^{ER\alpha/PGR}$ near genes highly expressed during diestrus; this was similar to estrus specific loops that overlapped common enhancers$^{ER\alpha/PGR}$ and could be either activation or repression as the loop was stable across the estrous cycle (Figure 5F). Stable loops also contained enhancer/promoter pairs from common enhancers^{other} and these were associated with both up- and downregulated DEGs, confirming activation and repression activity on gene expression in this group. Overlaps of the enhancer/promoter pairs in the three different loop categories with estradiol regulated DEGs showed the majority of gene expression changes correlated with gene expression direction 24 h after estrogen treatment (sustained) instead of 2 h (early) and would therefore impact gene expression at the next stage (Figure 5F and Supplementary Figure S9B). For example, a diestrus loop at a diestrus expressed gene would directly repress gene expression that occurred at estrus. Another example would be an estrus loop at an estrus expressed gene with direct repression that occurs at diestrus. These expression patterns would be most likely influenced by ERα/PGR for diestrus specific and common enhancers$^{ER\alpha/PGR}$ with promoter pairs and HIF2A for estrus specific and common enhancers^{other} with promoter pairs (Figure 5F and Supplementary Figure S9B).

Examples of these types of chromatin interactions and enhancer/promoter activity at DEGs are shown (Figure 5G). SMC1A ChIP-seq signal from the uterus of ovx mice is included for reference (51). *Rgs2* was a diestrus expressed gene with two diestrus specific loops around +50 kb and +90 kb of the *Rgs2* TSS (Figure 5G). Several diestrus specific enhancers were overlapped with the + 50kb loop end and several common enhancers$^{ER\alpha/PGR}$ were overlapped with the +90 kb loop end; all had diestrus specific ERα and PGR. Estrus specific loops were formed farther away from the *Rgs2* TSS than diestrus specific loops. The mode of activity for this gene appeared to be chromatin rearrangement to bring diestrus specific enhancers with ERα and PGR closer to the promoter to activate gene transcription during diestrus. Data from estradiol treatment of ovx mice, however, shows that it is actually acting as a repressor of gene transcription under the influence of ERα/PGR, resulting in lower expression during estrus.

Elf3 was an estrus expressed gene that had an estrus specific loop around +40 kb of the *Elf3* TSS (Figure 5G). This loop end contained two enhancer/promoter pairs (one estrus specific and one common enhancer^{other}). Another estrus specific loop, which did not directly link to the *Elf3* promoter, was located at +75 kb and looped to the +40 kb loop end, most likely bringing this region closer to the promoter during estrus. Loop ends near this gene generally lacked ERα and PGR but had estrus specific HIF2A. This finding, combined with HIF2A cKO data as well as estradiol treatment timing suggests that the mode of activity for this gene is estrus specific chromatin rearrangement that brings estrus specific enhancers with HIF2A closer to the promoter, repressing gene transcription that follows during diestrus.

A more complex example of these chromatin interactions was the enhancer/promoter pairs for the estrus expressed gene, *Wnt5a* (Figure 5G). During diestrus, there was a diestrus specific loop located −60 kb upstream of the *Wnt5a* TSS that overlapped two enhancer/promoter pairs (both common enhancers$^{ER\alpha/PGR}$). Another diestrus specific loop located at −50 kb to −130 kb of the *Wnt5a* TSS was in between that loop. The summary of this architecture would be diestrus specific accessibility with high levels of ERα and PGR that was brought closer to the *Wnt5a* promoter while *Wnt5a* gene expression was low suggesting activation that resulted in estrus expression. During estrus, several enhancer/promoter pairs appeared to be present (one estrus specific loop around -130kb and two common loops around −102 kb and −185 kb upstream of the *Wnt5a* TSS); all outside of the 100kb cutoff for enhancer/promoter pair identification (Figure 5G). These loop ends overlapped diestrus specific enhancers or common enhancers$^{ER\alpha/PGR}$. The summary of this activity was estrus specific distancing of enhancers from the promoter in combination with loss of accessibility, ERα and PGR that resulted in repression of *Wnt5a* during diestrus.

A final example is the estrus expressed gene, nucleic acid binding protein 1 (*Nabp1*), that demonstrates the proposed model of enhancer switching that was described in Figure 3F where gene expression relies on diestrus type enhancers during

diestrus that switch to an estrus type enhancer during estrus (Figure 5G). During diestrus there was a diestrus specific loop that overlapped a common enhancer$^{ER\alpha/PGR}$ located −52 kb upstream of the *Nabp1* promoter that had diestrus specific ERα and PGR; HIF2A was also found in this location but only during estrus. During estrus there was an estrus specific loop located at −32 kb upstream of the *Nabp1* promoter that overlapped a common enhancer^{other} that lacked ERα or PGR but had an estrus specific HIF2A. Increased gene expression during estrus was most likely controlled by ERα/PGR that was brought closer to the promoter during diestrus through chromatin looping. The loss of this ERα/PGR occupied loop combined with a switch to an estrus specific loop that overlapped an estrus type enhancer most likely resulted in loss of gene expression during diestrus.

Discussion

Here, we report the coordinated dynamics of uterine gene expression, chromatin accessibility and architecture, and TF binding during the mouse estrous cycle, a classic example of cyclic steroid hormone regulation. We anticipated that ERα would bind preferentially during diestrus (when estradiol is high) and PGR during estrus (when progesterone is high) but this was not the case. Instead, the primary mechanism of estrous cycle dependent gene expression control was through highly coordinated association of ERα and PGR together in complex during diestrus at diestrus specific or constitutively open enhancers; this association was lost during estrus (Figure 6). A secondary mechanism was constitutively open or estrus specific accessible enhancers that were independent of ERα/PGR and were most likely influenced by other TFs such as HIF2A; conditional uterine deletion of HIF2A confirmed its direct role in gene expression changes. The data strongly supports the idea that there is estrus cycle dependent switching between these two enhancer types to regulate individual genes. In addition to these two mechanisms, there were regions of limited accessibility that had either ERα or PGR bound during estrus; the function of these binding events is unknown. Chromatin looping was estrous cycle dependent and changes to enhancer/promoter pairs likely influenced gene expression. All these activities observed at enhancers were less pronounced at the TSS of target genes, apart from a few highly expressed genes where chromatin accessibility appeared to be the primary mechanism of control. These data demonstrate a highly orchestrated, dynamic interplay of transcription factors, chromatin accessibility and 3D structural rearrangements to control estrous cycle gene expression.

Estrous cycle dependent uterine gene expression changes primarily have been attributed to estradiol and progesterone-induced actions of their respective receptors, ERα and PGR. In adult ovx mice, ERα and PGR bind uterine chromatin in the absence of their ligands, but hormone treatment induces substantial, rapid increases in binding (6,29). We found that ERα and PGR ChIP-seq peaks from ovx mice treated with either estrogen or progesterone preferentially overlapped with our ERα and PGR ChIP-seq peaks during diestrus, but not estrus. This finding was unsurprising for ERα based on high estradiol levels during diestrus, and was consistent with estradiol/ERα-induced gene expression changes that result in the appropriate proteins being expressed during estrus, 30–36 hours later (38,55). The finding that progesterone-induced PGR ChIP-seq peaks in ovx mice had minimal overlap with estrus-associated PGR binding peaks was unexpected because progesterone levels are relatively high during estrus (2,3). These findings indicate that in the presence of endogenous estrogen and progesterone, PGR binding does not mirror progesterone levels (39). Based on our RIME data demonstrating direct association of ERα and PGR during diestrus, one influence on PGR binding is likely its interactions with ERα. These results highlight the complexity of hormone/receptor interactions in the physiological setting of the estrous cycle that cannot be captured using ovx models.

Dynamic TF occupancy at constitutively open chromatin influences gene expression (37,56,57). Similarly, we found that diestrus gene expression changes were most commonly associated with coordinated binding of ERα and PGR in constitutively open regions and in regions of chromatin with increased accessibility during diestrus. These regions contained EREs and PREs in close proximity as well as motifs of pioneering TFs including FOXA2, GATA and SOX. This finding was unsurprising because ERα interactions with pioneering TFs and coregulators such as chromatin remodelers, coactivators, and corepressors strongly influence estrogen signaling across estrogen-responsive cell and tissue types (11,58–61). In uterine cancer cells, estrogen treatment also exposes some progesterone dependent PGR binding sites that are required for both estrogen and progesterone driven gene expression (56). We speculate that in the cycling uterus, ERα and PGR facilitate each other's binding to increase chromatin accessibility at the regions that become more accessible during diestrus.

TFs can also bind chromatin at regions of relatively low accessibility as defined by ATAC-seq methods. ERα binds to these types of chromatin regions, even in the absence of ligand, in both breast cancer cells and whole uterine tissue (10,29). In breast cancer cells, PGR also binds to chromatin in the absence of ligand; however, locations that are PGR bound following progesterone treatment are typically highly accessible (57). We found that during estrus, most ERα and PGR binding was in locations of reduced chromatin accessibility. These regions were typically TF deserts but had some enrichment of PAX, ELK, ELF and EHF motifs. Notably, they did not have classical pioneer TF motifs such as FOXA, GATA or SOX, which were present in the constitutively open chromatin regions. In breast cancer cells, progesterone treatment induces direct interactions between PGR and ERα; this interaction appears to regulate sites of ERα binding and transcriptional output (49). This does not appear to be the case in the uterus during estrus because ERα and PGR were bound independently in estrus specific locations. The function of this estrus dependent ERα or PGR binding at relatively inaccessible chromatin is unclear.

An unexpected mode of estrous cycle gene expression control appeared to be either independent of ERα/PGR or only indirectly mediated by them. Estrus specific regions of accessibility had relatively low levels of ERα and PGR binding and minimal enrichment for ERE and PRE motifs. Instead, these regions had robust enrichment for HOX, PAX3/5/8, TEAD2/4, VDR and ETS family member motifs, suggesting that these TFs regulate gene expression during estrus (62). HOX genes, PAX genes and VDR are all required for the development and function of the female reproductive tract (63–65). ETS family members may be indirect targets of ERα and PGR through growth factor signaling pathways. In breast cancer cells, the growth factors EGF and bFGF induce ETS binding to its DNA response element, regulating target gene expression (66). Furthermore, EGF and IGF1 can act down-

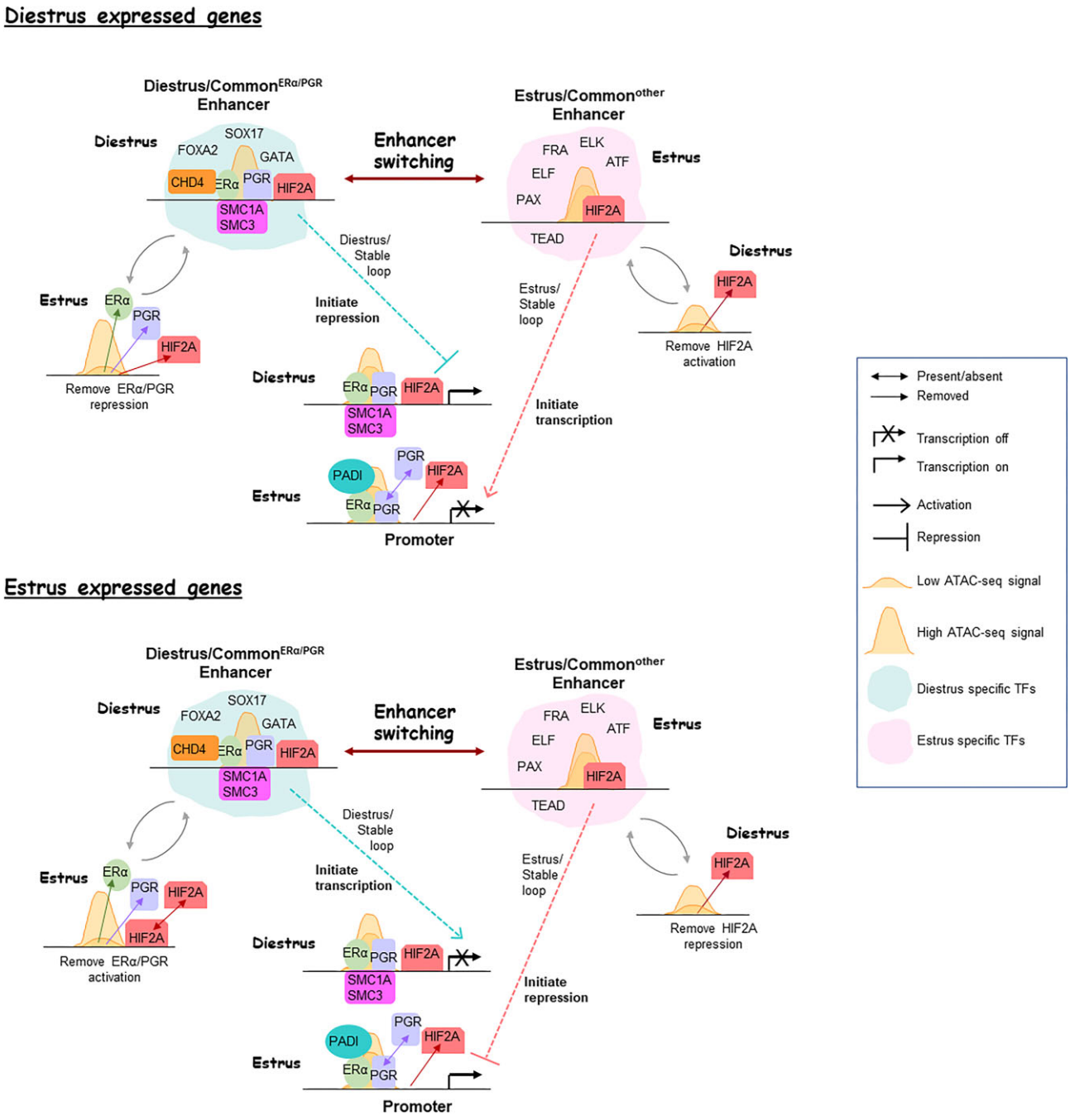

Figure 6. Model of estrous cycle dependent chromatin dynamics and transcription factor binding. Diestrus- and estrus-expressed genes are regulated by chromatin looping, accessibility changes, and transcription factor binding over the estrous cycle. Transcription factors included were either enriched motifs at DERs and DARs or binding partners of ERα as determined by RIME. Dashed lines indicate potential chromatin loops from enhancer/promoter pair analysis. ATAC-seq signal is indicated by height; increased accessibility = taller peak. The presence of two peaks for ATAC-seq indicates that either level of accessibility is possible. Diestrus- and estrus-expressed DEGs are predominantly characterized by enhancer switching from an ERα/PGR occupied enhancer during diestrus to a HIF2A occupied enhancer during estrus. Legend indicates symbol meaning.

stream of estrogen signaling and mimic estrogen induced proliferation and growth in the absence of estrogen (67–69). These data suggest that estrus specific regions of chromatin accessibility may be indirect targets of ERα/PGR signaling through induction of growth factor expression.

In addition to ETS family motifs, we found that estrus specific accessible chromatin had HIF1A/2A motifs and bound HIF2A. HIF1A and HIF2A coordinate gene expression changes in response to hypoxia by inducing changes in chromatin accessibility (70). HIF1A/2A binds preferentially to open chromatin in the presence of other transcription factors such as STAT3 and ELK; ELK1 and ELK4 (ETS family members) were also enriched motifs in estrus specific open chromatin. (71). Estrus specific accessibility may reveal otherwise hidden HIF binding sites, allowing HIF2A to bind in these locations. Growth factor and nutrient signaling stabilizes HIF alpha in the nucleus making it more available for chromatin binding (71). In breast cancer cells, hypoxia alters

expression of ERα target genes through changes in HIF1A/1B and modifies sites of ERα binding to chromatin (72). These cells also have hormone independent enhancer activation at genes with nearby HIF binding sites and reduced enrichment for EREs. In the mouse, conditional deletion of *Hif2a* in uterine stroma causes implantation failure, supporting a role for HIF2A in uterine responses to hormones (35). Here, a uterine conditional deletion of *Hif2a* confirmed its direct role in influencing about one quarter of estrous cycle gene expression changes and suggests HIF2A regulates gene expression towards diestrus expression patterns. Together, these findings suggest that HIF2A mediates some estrous cycle dependent chromatin accessibility and gene expression changes that are independent of direct ERα/PGR binding, perhaps through growth factor type signaling pathways.

Topologically associated chromatin domains (TADs) are relatively stable across cell types and have boundaries enriched for cohesins and CCCTC-binding factor (CTCF) binding (73). Within TADs, steroid hormone receptors influence chromatin accessibility in the absence and presence of hormones (56,74–79). For example, TADs can be regulated by 'hormone control regions', regions bound by ERα and PGR even in the absence of ligand, that form long range loops with hormone regulated target genes (74). Hormone exposure results in further rearrangement of chromatin within these regions and impacts expression of looped genes. These rearrangements do not appear to depend on CTCF binding because CTCF binding sites do not change much following hormone treatment. Similarly, we found diestrus specific loops that overlapped accessible chromatin occupied by ERα and PGR. However, we also found that cohesin complex proteins (SMC1A and SMC3) were in complex with ERα during diestrus, suggesting the possibility that ERα-cohesin interactions create stable chromatin loops without involving CTCF. In agreement, ovx mice exposed to estrogen have SMC1A binding sites that are enriched for EREs, potentially allowing for direct targeting of this complex to regions of ERα occupancy (51). However, estrogen treatment alone does not result in substantial differential looping in uterus from the ovx model, suggesting either the loops are preformed or they are not impacted by an acute exposure to estrogen in the absence of other hormones. The extensive chromatin rearrangements we observed across the estrous cycle support the latter interpretation.

In contrast to diestrus specific loops, estrus specific loops were characterized by low levels of ERα/PGR and estrus specific accessibility near genes that were highly expressed during estrus. This, combined with the lack of cohesin proteins in complex with ERα during estrus, suggested that other transcription factors such as HIF may be important for alterations in chromatin accessibility and/or loop formation. These chromatin changes occurred during estrus when estrogen levels are low, and were consistent with the observed enrichment of the HIF motif at SMC1A binding sites in ovx mice in the absence of estrogen (51). In breast cancer cells, HIF binds widely to the genome and increases accessibility in those locations under hypoxic conditions, but does not change the chromatin architecture, suggesting HIF itself does not influence chromatin structure in response to hypoxia (80). Unlike in breast cancer cells, HIF2A binding in the uterus was highly dynamic and coordinated with chromatin accessibility. This finding suggests that the cycling uterus depends on HIF2A binding to alter chromatin structure. Further studies of the factors that control both ERα/PGR dependent and ERα/PGR independent chromatin looping in the uterus in response to estrous cycle hormones will be important towards fully understanding gene expression control and the subsequent phenotypic outcomes.

Data availability

The sequencing data used in this study were deposited in the Gene Expression Omnibus database under accession code GSE234065 and are publicly available.

Supplementary data

Supplementary Data are available at NAR Online.

Acknowledgements

The authors would like to thank Sylvia Hewitt and H. K. Kinyamu from NIEHS for critical review of this manuscript. The authors would also like to thank the following NIEHS cores for their support: Epigenomics and DNA Sequencing Core Facility, Comparative Medicine Branch, and Cellular & Molecular Pathology Branch.

Funding

This research was supported by the Intramural Research Program of the National Institutes of Health, National Institute of Environmental Health Sciences [1ZIAES102405]. Funding for open access charge: NIEHS.

Conflict of interest statement

None declared.

References

1. Robertshaw,I., Bian,F. and Das,S.K. (2016) Mechanisms of uterine estrogen signaling during early pregnancy in mice: an update. *J. Mol. Endocrinol.*, **56**, R127–R138.
2. Nilsson,M.E., Vandenput,L., Tivesten,Å., Norlén,A.-K., Lagerquist,M.K., Windahl,S.H., Börjesson,A.E., Farman,H.H., Poutanen,M., Benrick,A., *et al.* (2015) Measurement of a comprehensive sex steroid profile in rodent serum by high-sensitive gas chromatography-tandem mass spectrometry. *Endocrinology*, **156**, 2492–2502.
3. Nelson,J.F., Felicio,L.S., Osterburg,H.H. and Finch,C.E. (1981) Altered profiles of estradiol and progesterone associated with prolonged estrous cycles and persistent vaginal cornification in aging C57BL/6J mice. *Biol. Reprod.*, **24**, 784–794.
4. Hewitt,S.C. and Korach,K.S. (2018) Estrogen receptors: new directions in the new millennium. *Endocr. Rev.*, **39**, 664–675.
5. Grimm,S.L., Hartig,S.M. and Edwards,D.P. (2016) Progesterone receptor signaling mechanisms. *J. Mol. Biol.*, **428**, 3831–3849.
6. Rubel,C.A., Lanz,R.B., Kommagani,R., Franco,H.L., Lydon,J.P. and DeMayo,F.J. (2012) Research resource: genome-wide profiling of progesterone receptor binding in the mouse uterus. *Mol. Endocrinol.*, **26**, 1428–1442.
7. Umesono,K. and Evans,R.M. (1989) Determinants of target gene specificity for steroid/thyroid hormone receptors. *Cell*, **57**, 1139–1146.
8. Clarke,C.L. and Graham,J.D. (2012) Non-overlapping progesterone receptor cistromes contribute to cell-specific transcriptional outcomes. *PLoS One*, **7**, 35859.

9. Jacobsen,B.M. and Horwitz,K.B. (2012) Progesterone receptors, their isoforms and progesterone regulated transcription. *Mol. Cell. Endocrinol.*, **357**, 18–29.
10. Chen,D., Parker,T.M., Bhat-Nakshatri,P., Chu,X., Liu,Y., Wang,Y. and Nakshatri,H. (2021) Nonlinear relationship between chromatin accessibility and estradiol-regulated gene expression. *Oncogene*, **40**, 1332–1346.
11. Magnani,L. and Lupien,M. (2014) Chromatin and epigenetic determinants of estrogen receptor alpha (ESR1) signaling. *Mol. Cell. Endocrinol.*, **382**, 633–641.
12. Westwood,F.R. (2008) The female rat reproductive cycle: a practical histological guide to staging. *Toxicol. Pathol.*, **36**, 375–384.
13. Trapnell,C., Pachter,L. and Salzberg,S.L. (2009) TopHat: discovering splice junctions with RNA-Seq. *Bioinforma. Orig. Pap.*, **25**, 1105–1111.
14. Trapnell,C., Williams,B., Pertea,G., Mortazavi,A., Kwan,G., van Baren,M.J., Salzberg,S.L., Wold,B.J. and Pachter,L. (2010) Transcript assembly and quantification by RNA-Seq reveals unannotated transcripts and isoform switching during cell differentiation. *Nat. Biotechnol.*, **28**, 511–515.
15. Yu,G., Wang,L.G., Han,Y. and He,Q.Y. (2012) ClusterProfiler: an R package for comparing biological themes among gene clusters. *Omi. A J. Integr. Biol.*, **16**, 284–287.
16. Winkler,I., Tolkachov,A., Lammers,F., Lacour,P., Daugelaite,K., Schneider,N., Koch,M.-L., Panten,J., Grünschläger,F., Poth,T., *et al.* (2024) The cycling and aging mouse female reproductive tract at single-cell resolution. *Cell*, **187**, 981–998.
17. Stuart,T., Butler,A., Hoffman,P., Hafemeister,C., Papalexi,E., Mauck,W.M., Hao,Y., Stoeckius,M., Smibert,P. and Satija,R. (2019) Comprehensive integration of single-cell Data. *Cell*, **177**, 1888–1902.
18. Padilla-Banks,E., Jefferson,W.N., Papas,B.N., Suen,A.A., Xu,X., Carreon,D.V., Willson,C.J., Quist,E.M. and Williams,C.J. (2023) Developmental estrogen exposure in mice disrupts uterine epithelial cell differentiation and causes adenocarcinoma via Wnt/β-catenin and PI3K/AKT signaling. *PLoS Biol.*, **21**, e3002334.
19. Langmead,B., Trapnell,C., Pop,M. and Salzberg,S.L. (2009) Ultrafast and memory-efficient alignment of short DNA sequences to the human genome. *Genome Biol.*, **10**, R25.
20. Raney,B.J., Barber,G.P., Benet-Pagès,A., Casper,J., Clawson,H., Cline,M.S., Diekhans,M., Fischer,C., Navarro Gonzalez,J., Hickey,G., *et al.* (2024) The UCSC genome browser database: 2024 update. *Nucleic Acids Res.*, **52**, D1082–D1088.
21. Zhang,Y., Liu,T., Meyer,C.A., Eeckhoute,J., Johnson,D.S., Bernstein,B.E., Nusbaum,C., Myers,R.M., Brown,M., Li,W., *et al.* (2008) Model-based analysis of ChIP-Seq (MACS). *Genome Biol.*, **9**, R137.
22. Buenrostro,J.D., Wu,B., Chang,H.Y. and Greenleaf,W.J. (2015) ATAC-seq: a method for assaying chromatin accessibility genome-wide. *Curr. Protoc. Mol. Biol.*, **109**, 21.29.1–21.29.9.
23. Corces,M.R., Trevino,A.E., Hamilton,E.G., Greenside,P.G., Sinnott-Armstrong,N.A., Vesuna,S., Satpathy,A.T., Rubin,A.J., Montine,K.S., Wu,B., *et al.* (2017) An improved ATAC-seq protocol reduces background and enables interrogation of frozen tissues. *Nat. Methods*, **14**, 959–962.
24. Heinz,S., Benner,C., Spann,N., Bertolino,E., Lin,Y.C., Laslo,P., Cheng,J.X., Murre,C., Singh,H. and Glass,C.K. (2010) Simple combinations of lineage-determining transcription factors prime cis-regulatory elements required for macrophage and B cell identities. *Mol. Cell*, **38**, 576–589.
25. Lienhard,M., Grimm,C., Morkel,M., Herwig,R. and Chavez,L. (2014) MEDIPS: genome-wide differential coverage analysis of sequencing data derived from DNA enrichment experiments. *Bioinformatics*, **30**, 284–286.
26. Wingett,S.W., Ewels,P., Furlan-Magaril,M., Nagano,T., Schoenfelder,S., Fraser,P. and Andrews,S. (2015) HiCUP: pipeline for mapping and processing Hi-C data. *F1000Research*, **4**, 1310.
27. Durand,N.C., Shamim,M.S., Machol,I., Rao,S.S.P., Huntley,M.H., Lander,E.S. and Aiden,E.L. (2016) Juicer provides a one-click system for analyzing loop-resolution Hi-C experiments. *Cell Syst.*, **3**, 95–98.
28. Mohammed,H., D'Santos,C., Serandour,A.A., Ali,H.R., Brown,G.D., Atkins,A., Rueda,O.M., Holmes,K.A., Theodorou,V., Robinson,J.L.L., *et al.* (2013) Endogenous purification reveals GREB1 as a key estrogen receptor regulatory factor. *Cell Rep.*, **3**, 342–349.
29. Hewitt,S.C., Li,L., Grimm,S.A., Chen,Y., Liu,L., Li,Y., Bushel,P.R., Fargo,D. and Korach,K.S. (2012) Research resource: whole-genome estrogen receptor α binding in mouse uterine tissue revealed by ChIP-Seq. *Mol. Endocrinol.*, **26**, 887–898.
30. Collins,J.M., Huo,Z. and Wang,D. (2021) ESR1 ChIP-Seq identifies distinct ligand-free ESR1 genomic binding sites in human hepatocytes and liver tissue. *Int. J. Mol. Sci.*, **22**, 1461.
31. Filant,J., Lydon,J.P. and Spencer,T.E. (2014) Integrated chromatin immunoprecipitation sequencing and microarray analysis identifies FOXA2 target genes in the glands of the mouse uterus. *FASEB J.*, **28**, 230–243.
32. Rubel,C.A., Wu,S.-P., Lin,L., Wang,T., Lanz,R.B., Li,X., Kommagani,R., Franco,H.L., Camper,S.A., Tong,Q., *et al.* (2016) A Gata2-dependent transcription network regulates uterine progesterone responsiveness and endometrial function. *Cell Rep.*, **17**, 1414–1425.
33. Vasquez,Y.M., Wang,X., Wetendorf,M., Franco,H.L., Mo,Q., Wang,T., Lanz,R.B., Young,S.L., Lessey,B.A., Spencer,T.E., *et al.* (2018) FOXO1 regulates uterine epithelial integrity and progesterone receptor expression critical for embryo implantation. *PLoS Genet.*, **14**, e1007787.
34. Dinh,D.T., Breen,J., Akison,L.K., DeMayo,F.J., Brown,H.M., Robker,R.L. and Russell,D.L. (2019) Tissue-specific progesterone receptor-chromatin binding and the regulation of progesterone-dependent gene expression. *Sci. Rep.*, **9**, 11966.
35. Matsumoto,L., Hirota,Y., Saito-Fujita,T., Takeda,N., Tanaka,T., Hiraoka,T., Akaeda,S., Fujita,H., Shimizu-Hirota,R., Igaue,S., *et al.* (2018) HIF2a in the uterine stroma permits embryo invasion and luminal epithelium detachment. *J. Clin. Invest.*, **128**, 3186–3197.
36. Bhurke,A., Kannan,A., Neff,A., Ma,Q., Laws,M.J., Taylor,R.N., Bagchi,M.K. and Bagchi,I.C. (2020) A hypoxia-induced Rab pathway regulates embryo implantation by controlled trafficking of secretory granules. *Proc. Natl. Acad. Sci. U.S.A.*, **117**, 14532–14542.
37. Klemm,S.L., Shipony,Z. and Greenleaf,W.J. (2019) Chromatin accessibility and the regulatory epigenome. *Nat. Rev. Genet.*, **20**, 207–220.
38. Winuthayanon,W., Hewitt,S.C. and Korach,K.S. (2014) Uterine epithelial cell estrogen receptor alpha-dependent and -independent genomic profiles that underlie estrogen responses in mice. *Biol. Reprod.*, **91**, 110.
39. Kommagani,R., Szwarc,M.M., Kovanci,E., Creighton,C.J., O'Malley,B.W., Demayo,F.J. and Lydon,J.P. (2014) A murine uterine transcriptome, responsive to steroid receptor coactivator-2, reveals transcription factor 23 as essential for decidualization of human endometrial stromal cells. *Biol. Reprod.*, **90**, 75.
40. Franco,H.L., Lee,K.Y., Broaddus,R.R., White,L.D., Lanske,B., Lydon,J.P., Jeong,J.-W. and DeMayo,F.J. (2010) Ablation of Indian hedgehog in the murine uterus results in decreased cell cycle progression, aberrant epidermal growth factor signaling, and increased estrogen signaling. *Biol. Reprod.*, **82**, 783–790.
41. Massé,J., Watrin,T., Laurent,A., Deschamps,S., Guerrier,D. and Pellerin,I. (2009) The developing female genital tract: from genetics to epigenetics. *Int. J. Dev. Biol.*, **53**, 411–424.
42. Jefferson,W.N., Karimi Kinyamu,H., Wang,T., Miranda,A.X., Padilla-Banks,E., Suen,A.A. and Williams,C.J. (2018) Widespread enhancer activation via ERα mediates estrogen response in vivo during uterine development. *Nucleic Acids Res.*, **46**, 5487–5503.
43. Kawai,H., Li,H., Avraham,S., Jiang,S. and Avraham,H.K. (2003) Overexpression of histone deacetylase HDAC1 modulates breast

cancer progression by negative regulation of estrogen receptor α. *Int. J. Cancer*, **107**, 353–358.
44. Le Romancer,M., Treilleux,I., Leconte,N., Robin-Lespinasse,Y., Sentis,S., Bouchekioua-Bouzaghou,K., Goddard,S., Gobert-Gosse,S. and Corbo,L. (2008) Regulation of estrogen rapid signaling through arginine methylation by PRMT1. *Mol. Cell*, **31**, 212–221.
45. Marques,J.G., Gryder,B.E., Pavlovic,B., Chung,Y., Ngo,Q.A., Frommelt,F., Gstaiger,M., Song,Y., Benischke,K., Laubscher,D., *et al.* (2020) NURD subunit CHD4 regulates super-enhancer accessibility in rhabdomyosarcoma and represents a general tumor dependency. *eLife*, **9**, e54993.
46. Zhang,X., Bolt,M., Guertin,M.J., Chen,W., Zhang,S., Cherrington,B.D., Slade,D.J., Dreyton,C.J., Subramanian,V., Bicker,K.L., *et al.* (2012) Peptidylarginine deiminase 2-catalyzed histone H3 arginine 26 citrullination facilitates estrogen receptor target gene activation. *Proc. Natl. Acad. Sci. U.S.A.*, **109**, 13331–13336.
47. Guertin,M.J., Zhang,X., Anguish,L., Kim,S., Varticovski,L., Lis,J.T., Hager,G.L. and Coonrod,S.A. (2014) Targeted H3R26 deimination specifically facilitates estrogen receptor binding by modifying nucleosome structure. *PLoS Genet.*, **10**, e1004613.
48. Li,Z., Zhang,Y., Hedman,A.C., Ames,J.B. and Sacks,D.B. (2017) Calmodulin lobes facilitate dimerization and activation of estrogen receptor-α. *J. Biol. Chem.*, **292**, 4614–4622.
49. Mohammed,H., Russell,I.A., Stark,R., Rueda,O.M., Hickey,T.E., Tarulli,G.A., Serandour,A.A., Birrell,S.N., Bruna,A., Saadi,A., *et al.* (2015) Progesterone receptor modulates ERα action in breast cancer. *Nature*, **523**, 313–317.
50. Siersbæk,R., Scabia,V., Nagarajan,S., Chernukhin,I., Papachristou,E.K., Broome,R., Johnston,S.J., Joosten,S.E.P., Green,A.R., Kumar,S., *et al.* (2020) IL6/STAT3 signaling hijacks estrogen receptor α enhancers to drive breast cancer metastasis. *Cancer Cell*, **38**, 412–423.
51. Hewitt,S.C., Grimm,S.A., Wu,S.P., DeMayo,F.J. and Korach,K.S. (2020) Estrogen receptor α (ERα)-binding super-enhancers drive key mediators that control uterine estrogen responses in mice. *J. Biol. Chem.*, **295**, 8387–8400.
52. Mumbach,M.R., Rubin,A.J., Flynn,R.A., Dai,C., Khavari,P.A., Greenleaf,W.J. and Chang,H.Y. (2016) HiChIP: efficient and sensitive analysis of protein-directed genome architecture. *Nat. Methods*, **13**, 919–922.
53. Zhang,T., Zhang,Z., Dong,Q., Xiong,J. and Zhu,B. (2020) Histone H3K27 acetylation is dispensable for enhancer activity in mouse embryonic stem cells. *Genome Biol.*, **21**, 45.
54. Pradeepa,M.M. (2017) Causal role of histone acetylations in enhancer function. *Transcription*, **8**, 40–47.
55. Ajayi,A.F. and Akhigbe,R.E. (2020) Staging of the estrous cycle and induction of estrus in experimental rodents: an update. *Fertil. Res. Pract.*, **6**, 5.
56. La Greca,A., Bellora,N., Le Dily,F., Jara,R., Nacht,A.S., Quilez Oliete,J., Villanueva,J.L., Vidal,E., Merino,G., Fresno,C., *et al.* (2022) Chromatin topology defines estradiol-primed progesterone receptor and PAX2 binding in endometrial cancer cells. *eLife*, **11**, e66034.
57. Zaurin,R., Ferrari,R., Nacht,A.S., Carbonell,J., Le Dily,F., Font-Mateu,J., Cucalon,L.I., de,L., Vidal,E., Lioutas,A., *et al.* (2021) A set of accessible enhancers enables the initial response of breast cancer cells to physiological progestin concentrations. *Nucleic Acids Res.*, **49**, 12716.
58. Carroll,J.S., Liu,X.S., Brodsky,A.S., Li,W., Meyer,C.A., Szary,A.J., Eeckhoute,J., Shao,W., Hestermann,E.V., Geistlinger,T.R., *et al.* (2005) Chromosome-wide mapping of estrogen receptor binding reveals long-range regulation requiring the forkhead protein FoxA1. *Cell*, **122**, 33–43.
59. Seachrist,D.D., Anstine,L.J. and Keri,R.A. (2021) FOXA1: a pioneer of nuclear receptor action in breast cancer. *Cancer*, **13**, 5205.
60. Zhang,Y., Zhang,Y., Chan,H.L., Chan,H.L., Garcia-Martinez,L., Garcia-Martinez,L., Karl,D.L., Weich,N., Weich,N., Slingerland,J.M., *et al.* (2020) Estrogen induces dynamic ERα and RING1B recruitment to control gene and enhancer activities in luminal breast cancer. *Sci. Adv.*, **6**, 7249–7254.
61. Manavathi,B., Samanthapudi,V.S.K. and Gajulapalli,V.N.R. (2014) Estrogen receptor coregulators and pioneer factors: the orchestrators of mammary gland cell fate and development. *Front. Cell Dev. Biol.*, **2**, 34.
62. Dhara,A., Ghosh,S. and Sen,N. (2022) Regulation of ETS family of transcription factors in cancer. *J. Cancer Biol.*, **3**, 33–49.
63. Mittag,J., Winterhager,E., Bauer,K. and Grümmer,R. (2007) Congenital hypothyroid female Pax8-deficient mice are infertile despite thyroid hormone replacement therapy. *Endocrinology*, **148**, 719–725.
64. Yoshizawa,T., Handa,Y., Uematsu,Y., Takeda,S., Sekine,K., Yoshihara,Y., Kawakami,T., Arioka,K., Sato,H., Uchiyama,Y., *et al.* (1997) Mice lacking the vitamin D receptor exhibit impaired bone formation, uterine hypoplasia and growth retardation after weaning. *Nat. Genet.*, **16**, 391–396.
65. Du,H. and Taylor,H.S. (2016) The role of Hox genes in female reproductive tract development, adult function, and fertility. *Cold Spring Harb. Perspect. Med.*, **6**, a023002.
66. Myers,E., Hill,A.D.K., Kelly,G., McDermott,E.W., O'Higgins,N.J., Buggy,Y. and Young,L.S. (2005) Associations and interactions between Ets-1 and Ets-2 and coregulatory proteins, SRC-1, AIB1, and NCoR in breast cancer. *Clin. Cancer Res.*, **11**, 2111–2122.
67. Hewitt,S.C., Li,Y., Li,L. and Korach,K.S. (2010) Estrogen-mediated regulation of Igf1 transcription and uterine growth involves direct binding of estrogen receptor α to estrogen-responsive elements. *J. Biol. Chem.*, **285**, 2676–2685.
68. Hewitt,S.C., Lierz,S.L., Garcia,M., Hamilton,K.J., Gruzdev,A., Grimm,S.A., Lydon,J.P., Demayo,F.J. and Korach,K.S. (2019) A distal super enhancer mediates estrogen-dependent mouse uterine–specific gene transcription of Igf1 (insulin-like growth factor 1). *J. Biol. Chem.*, **294**, 9746–9759.
69. Nelson,K.G., Takahashi,T., Bossert,N.L., Walmert,D.K. and Mclachlan,J.A. (1991) Epidermal growth factor replaces estrogen in the stimulation of female genital-tract growth and differentiation (uterus/vagina/DNA synthesis). *Proc. Nati. Acad. Sci. U.S.A.*, **88**, 21–25.
70. Batie,M., Frost,J., Shakir,D. and Rocha,S. (2022) Regulation of chromatin accessibility by hypoxia and HIF. *Biochem. J.*, **479**, 767–786.
71. Dengler,V.L., Galbraith,M. and Espinosa,J.M. (2014) Transcriptional regulation by hypoxia inducible factors. *Crit. Rev. Biochem. Mol. Biol.*, **49**, 1–15.
72. Jehanno,C., Le Goff,P., Habauzit,D., Le Page,Y., Lecomte,S., Lecluze,E., Percevault,F., Avner,S., Métivier,R., Michel,D., *et al.* (2022) Hypoxia and ERα transcriptional crosstalk is associated with endocrine resistance in breast cancer. *Cancers (Basel)*, **14**, 4934.
73. Schoenfelder,S. and Fraser,P. (2019) Long-range enhancer–promoter contacts in gene expression control. *Nat. Rev. Genet.*, **20**, 437–455.
74. Le Dily,F., Vidal,E., Cuartero,Y., Quilez,J., Nacht,A.S., Vicent,G.P., Carbonell-Caballero,J., Sharma,P., Villanueva-Cañas,J.L., Ferrari,R., *et al.* (2019) Hormone-control regions mediate steroid receptor–dependent genome organization. *Genome Res.*, **29**, 29–39.
75. Le Dily,F.L., Baù,D., Pohl,A., Vicent,G.P., Serra,F., Soronellas,D., Castellano,G., Wright,R.H.G., Ballare,C., Filion,G., *et al.* (2014) Distinct structural transitions of chromatin topological domains correlate with coordinated hormone-induced gene regulation. *Genes Dev.*, **28**, 2151–2162.
76. Nuñez-Olvera,S.I., Puente-Rivera,J., Ramos-Payán,R., Pérez-Plasencia,C., Salinas-Vera,Y.M., Aguilar-Arnal,L. and López-Camarillo,C. (2021) Three-dimensional genome organization in breast and gynecological cancers: how chromatin folding influences tumorigenic transcriptional programs. *Cells*, **11**, 75.

77. Achinger-Kawecka,J., Valdes-Mora,F., Luu,P.-L., Giles,K.A., Caldon,C.E., Qu,W., Nair,S., Soto,S., Locke,W.J., Yeo-Teh,N.S., *et al.* (2020) Epigenetic reprogramming at estrogen-receptor binding sites alters 3D chromatin landscape in endocrine-resistant breast cancer. *Nat. Commun.*, **11**, 320.
78. Stavreva,D.A. and Hager,G.L. (2015) Chromatin structure and gene regulation: a dynamic view of enhancer function. *Nucleus*, **6**, 442–448.
79. Mourad,R., Hsu,P.-Y., Juan,L., Shen,C., Koneru,P., Lin,H., Liu,Y., Nephew,K., Huang,T.H. and Li,L. (2014) Estrogen induces global reorganization of chromatin structure in human breast cancer cells. *PLoS One*, **9**, e113354.
80. Platt,J.L., Salama,R., Smythies,J., Choudhry,H., Davies,J.O., Hughes,J.R., Ratcliffe,P.J. and Mole,D.R. (2016) Capture-C reveals preformed chromatin interactions between HIF-binding sites and distant promoters. *EMBO Rep.*, **17**, 1410–1421.

Received: January 15, 2024. **Revised:** June 27, 2024. **Editorial Decision:** July 27, 2024. **Accepted:** August 6, 2024
Published by Oxford University Press on behalf of Nucleic Acids Research 2024.